JBC RESEARCH ARTICLE

Lipidated peptides derived from intracellular loops 2 and 3 of the urotensin II receptor act as biased allosteric ligands

Received for publication, November 23, 2020, and in revised form, July 23, 2021 Published, Papers in Press, August 10, 2021,
https://doi.org/10.1016/j.jbc.2021.101057

Hassan Nassour[1,‡], Tuan Anh Hoang[1,‡], Ryan D. Martin[2], Juliana C. C. Dallagnol[1,2,3], Étienne Billard[1,2], Myriam Létourneau[1], Ettore Novellino[4], Alfonso Carotenuto[4], Bruce G. Allen[3], Jason C. Tanny[2], Alain Fournier[1], Terence E. Hébert[2], and David Chatenet[1,*]

From the [1]Institut National de la Recherche Scientifique, Centre Armand-Frappier Santé Biotechnologie, Groupe de Recherche en Ingénierie des Peptides et en Pharmacothérapie (GRIPP), Université du Québec, Ville de Laval, Québec, Canada; [2]Department of Pharmacology and Therapeutics, McGill University, Montreal, Québec, Canada; [3]Department of Medicine, Université de Montreal, Montreal Heart Institute, Montreal, Québec, Canada; and [4]Department of Pharmacy, University of Naples "Federico II", Naples, Italy

Edited by Henrik Dohlman

Over the last decade, the urotensinergic system, composed of one G protein-coupled receptor and two endogenous ligands, has garnered significant attention as a promising new target for the treatment of various cardiovascular diseases. Indeed, this system is associated with various biomarkers of cardiovascular dysfunctions and is involved in changes in cardiac contractility, fibrosis, and hypertrophy contributing, like the angiotensinergic system, to the pathogenesis and progression of heart failure. Significant investment has been made toward the development of clinically relevant UT ligands for therapeutic intervention, but with little or no success to date. This system therefore remains to be therapeutically exploited. Pepducins and other lipidated peptides have been used as both mechanistic probes and potential therapeutics; therefore, pepducins derived from the human urotensin II receptor might represent unique tools to generate signaling bias and study hUT signaling networks. Two hUT-derived pepducins, derived from the second and the third intracellular loop of the receptor (hUT-Pep2 and [Trp^1, Leu^2]hUT-Pep3, respectively), were synthesized and pharmacologically characterized. Our results demonstrated that hUT-Pep2 and [Trp^1, Leu^2]hUT-Pep3 acted as biased ago-allosteric modulators, triggered $ERK_{1/2}$ phosphorylation and, to a lesser extent, IP_1 production, and stimulated cell proliferation yet were devoid of contractile activity. Interestingly, both hUT-derived pepducins were able to modulate human urotensin II (hUII)- and urotensin II-related peptide (URP)-mediated contraction albeit to different extents. These new derivatives represent unique tools to reveal the intricacies of hUT signaling and also a novel avenue for the design of allosteric ligands selectively targeting hUT signaling potentially.

In humans, the urotensinergic system, composed of a class 1A G protein-coupled receptor (GPCR, hUT), and two endogenous peptide ligands, urotensin II (UII; hUII = H-Glu-Thr-Pro-Asp-c[Cys-Phe-Trp-Lys-Tyr-Cys]-Val-OH) and urotensin II-related peptide (URP, H-Ala-c[Cys-Phe-Trp-Lys-Tyr-Cys]-Val-OH), continues to represent a promising target for the treatment of several pathologies (1, 2). Notably, multiple studies in animal models have suggested that UT antagonists may represent potential therapeutic agents for treating atherosclerosis (3–6), pulmonary arterial hypertension (7–9), metabolic syndrome (4), and heart failure (10–12). However, in spite of such promise, clinical studies of UT candidate antagonists have had limited success due to a lack of efficacy in humans (1, 2, 13, 14). Our current knowledge remains insufficient to clearly assess its therapeutic potential, and accordingly, a deeper understanding of UT pharmacology is critically needed to accelerate development of UT ligands exhibiting efficacy in humans.

While the two endogenous ligands share a common bioactive core, the distinct N-terminal domain of UII isoforms appears to be involved in specific topological changes associated with UT activation (2, 15–17). Contingent on their interactions with UT, UII and URP probably induce distinct UT conformational changes that lead to divergent signaling profiles with both common and distinct biological activities (2, 17–21). Recent years have witnessed the emergence of useful molecules, with probe-dependent actions, that could shed light on the respective roles and importance of UII and URP under normal and pathological conditions (13, 17, 18, 22–27).

Promoting specific GPCR signaling events with biased agonists or allosteric modulators is a potentially innovative way to treat numerous conditions including cardiovascular disease, diabetes as well as neuropsychiatric/neurodegenerative disorders (28). Hence, this notion has been introduced into various drug discovery programs through theoretical predictions based on known signaling components of cells and from studies in knockout animals (reviewed in (29)). However, there are numerous instances where it is still not yet possible to predict what type of signaling bias represents a superior therapeutic approach. In these cases, empirical testing of exemplar molecules in animal models is a way forward. Such tools are

‡ These authors contributed equally to this work.
* For correspondence: David Chatenet, david.chatenet@iaf.inrs.ca.

currently unavailable in the context of the urotensinergic system.

Pepducins are lipidated cell-penetrating peptides composed of a lipid moiety attached to a peptide corresponding to an amino acid segment from one of the cytoplasmic loops of a GPCR of interest (reviewed in (30, 31)). Following establishment of an equilibrium between the inner and outer leaflets of the lipid bilayer, pepducins interact with their cognate GPCR leading to stabilization of a restricted subset of its inactive and active conformational states (32–34). Hence, such compounds can function as allosteric agonists or positive/negative allosteric modulators, making them useful for the study of GPCR signaling, as reported for protease-activated receptors (33, 34), chemokine receptors (35, 36), and β-adrenergic receptors (37), as well as for the potential treatment of various diseases including inflammatory diseases, cardiovascular pathologies, and cancer (38).

Here, we describe the design and pharmacological characterization of two pepducins derived from the second (hUT-Pep2) and third ([Trp^1, Leu^2]hUT-Pep3) intracellular loops of hUT. Our results demonstrate that both hUT-derived pepducins, while noncytotoxic, mediate $ERK_{1/2}$ phosphorylation and IP_1 accumulation. Using BRET-based biosensors, we observed that [Trp^1, Leu^2]hUT-Pep3 induced G_q, G_i, G_{13}, β-arrestin 1, β-arrestin 2 activation, and epidermal growth factor receptor (EGFR) transactivation while UT-Pep2 only activated G_i, G_{13}, β-arrestin-2 and EGFR transactivation. Interestingly, while only [Trp^1, Leu^2]hUT-Pep3 was able to induce proliferation in HEK 293-hUT cells, both pepducins were able to cause proliferation of neonatal rat cardiac fibroblasts. Further, while both hUT-derived pepducins were unable to induce rat aortic ring contraction on their own, they could modulate hUII- and URP-mediated contraction to different extents. These new molecular tools represent unique UT-targeted ligands that can be used to interrogate the involvement of specific pathways in hUT-associated diseases and to develop pharmacological agents with fewer side effects and a unique and more precise action for the treatment of various pathologies.

Results

Design and toxicity testing of hUT-derived pepducins

Pepducins are composed of a synthetic peptide, mimicking an intracellular GPCR loop, to which a hydrophobic moiety, most commonly the fully saturated C_{16} fatty acid palmitate, is conjugated at their N-termini (39). Based on a predicted structure for hUT (14, 15), pepducins derived from the sequence of hUT intracellular loops 2 and 3 (Table 1) were synthesized using solid-phase peptide synthesis. hUT-Pep2 is identical to the ICL2 sequence found in hUT. The second pepducin ([Trp^1, Leu^2]hUT-Pep3) comprises the hUT ICL3 sequence; however, the first two N-terminal amino acids were replaced by the corresponding residues from rat UT ICL3 (-Arg-Arg-in hUT and -Trp-Leu- in rUT). This modification was necessary since the pepducin derived from hUT ICL3, comprising seven positively charged residues, was highly cytotoxic from 10^{-7} M, which prevented further use (Fig. 1*A*). Nonetheless, hUT-Pep2 and [Trp^1, Leu^2]hUT-Pep3, up to 10^{-5} M, did not significantly affect HEK 293 cell viability (Fig. 1*A*). However, at 10^{-4} M, both derivatives were as cytotoxic as unmodified hUT-Pep3 at 10^{-7} M. Since these derivatives translocate to the inner leaflet of the plasma membrane, we tested the possibility that they promoted LDH release into the culture media. As shown in Figure 1*B*, none of these compounds, tested at the highest concentration (10^{-5} M) that did not lead to cell death, triggered LDH release. Altogether, our results demonstrated that both pepducins did not reduce cell viability at the concentrations used. Similar results were obtained in a second stably transfected CHO-hUT cell line (data not shown).

hUT-Pep2 and [Trp^1, Leu^2]hUT-Pep3 conserve a structure similar to as seen in the full-length receptor

Conformational analysis of hUT-Pep2 and [Trp^1, Leu^2]hUT-Pep3 was performed using solution NMR in DPC micelle suspensions, a solvent system commonly used in NMR and CD studies to mimic the zwitterionic membrane environment (40). Figures of the NOESY spectra of hUT-Pep2 and [Trp^1, Leu^2]hUT-Pep3 are shown in the supporting information (Figs. S1 and S2). hUT-Pep2 yielded well-resolved NMR spectra and measured NMR parameters indicated a folded structure (Tables S1 and S2). In particular, medium-range Nuclear Overhauser effects (NOEs, Table S2) between Hα(i) and HN(i+2) pointed to β-turn structures confirmed by other diagnostic parameters, such as amide temperature coefficients and $^3J_{HN\text{-}HA}$ coupling constants. The palmitate moiety turned out to be mostly unstructured, as could be inferred by the degeneracy of the proton chemical shifts of almost all the

Table 1
Amino acid sequences and analytical data of compounds hUII, URP, and hUT-derived pepducins

Cpd name	Sequence	MW[a] calc	MS[b] found
hUII	H-Glu-Thr-Pro-Asp-[Cys-Phe-Trp-Lys-Tyr-Cys]-Val-OH	1387.6	1388.1
URP	H-Ala-[Cys-Phe-Trp-Lys-Tyr-Cys]-Val-OH	1016.4	1016.4
hUT-Pep2	Palm-Arg-Pro-Leu-Asp-Thr-Val-Gln-Arg-Pro-Lys-Gly-Tyr-NH_2	1666.0	1667.1
[Trp^1, Leu^2]hUT-Pep3	Palm-Trp-Leu-Ser-Gln-Arg-Ala-Ser-Phe-Lys-Arg-Ala-Arg-Arg-NH_2	1899.3	1899.9

Abbreviation: Palm, palmitoyl.
Values represent the observed m/z of the monoisotope $[M + H]^+$ ions.
[a] Molecular weight calculated on a CEM Liberty Blue peptide synthesizer software.
[b] MALDI-TOF mass spectral analysis (m/z).

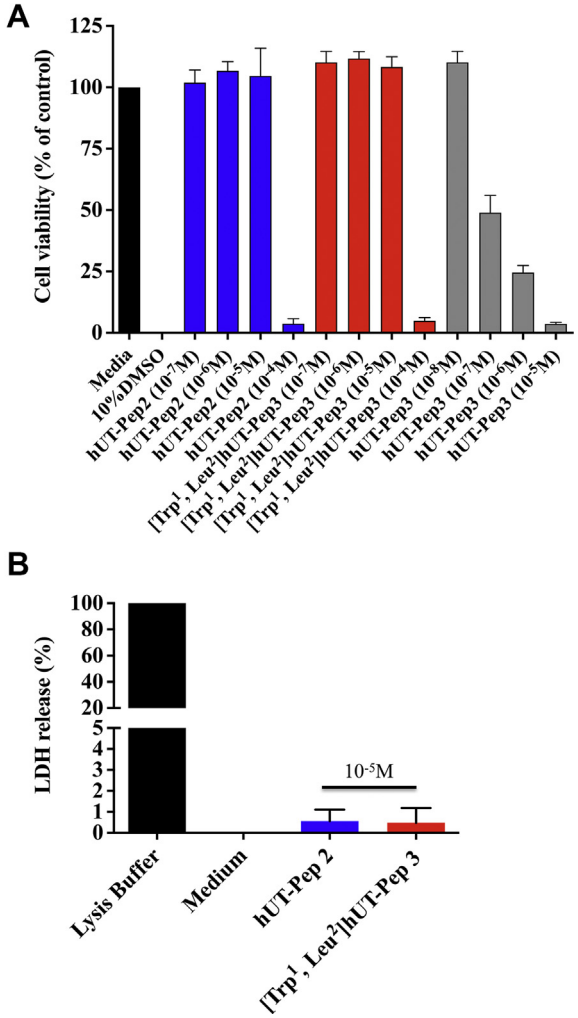

Figure 1. Cytotoxic action of hUT-pepducins. Toxicity of hUT-derived pepducins was evaluated using (*A*) MTT or (*B*) LDH assays in HEK 293-hUT cells.

methylene groups. However, the amide bond connecting palmitate and peptide is in *trans* configuration as suggested by the intense NOE contact between the Cα protons of the palmitate and NH of Arg^1. Actually, 135 NOEs (Table S2) were used in the structure calculation of hUT-Pep2, which corresponds to 11.2 NOEs per residue, a ratio similar to what is found in structured protein (41). Among those, 22 medium range NOEs in line with folded (β-turn) peptides were observed. Restrained MD calculations provided the well-defined structures shown in Figure 2*A*. Starting from the N-terminus, two type I β-turns along residues 1–4 and 3–6 and three distorted (type IV) β-turns along residues 4–7, 5–8, and 6–9 can be observed in the simulated structures of hUT-Pep2. Interestingly, the obtained structure can be easily overlapped with the corresponding ICL2 segment of a hUT model recently generated (Fig. 2*B*) (15). hUT-Pep2 therefore preserves the conformational propensities of the corresponding ICL2 segment when embedded in the wild-type receptor. Unfortunately, NMR spectra of [Trp^1, Leu^2]hUT-Pep3, despite complete assignment of all the proton resonances (Table S3), showed many broad and overlapping signals particularly in the amide proton region that prevented measure of many NMR parameters ($^3J_{HN\text{-}HA}$ coupling constants and most of the NOEs), and therefore NMR-based calculation of its 3D structure. However, retrievable NMR parameters from the spectra (a few NOEs, up-field shifts of the Hα resonances, and amide temperature coefficients, Tables S3 and S4) suggest a high tendency of [Trp^1, Leu^2]hUT-Pep3 to fold into a helix. Using circular dichroism (CD) analyses, we were able to observe that [Trp^1, Leu^2]hUT-Pep3, under any condition tested, was able to assume folded structural motifs (Fig. 2*C*). In 0.1 mg mL^{-1} SDS solution (red), it appeared to assume a β-sheet conformation (lower peak at 216 nm), while in TFE solutions it appeared to fold as an α-helix (dark green, TFE 80%, lower peaks at 205 and 216 nm). In 0.5 mg mL^{-1} DPC solution, it appeared to assume a less structured α-helix conformation, which correlates with our NMR data, while in water a nonstructured shape (random coil) was adopted. Worth noting, a pepducin derived from the ICL3 of PAR1 studied in DPC solutions also showed a stable helical conformation (42). Together, these results suggest that both pepducins likely adopt conformations closely related to those found within the wild-type receptor.

hUT-derived pepducins generate IP_1 production

hUT-mediated production of the inositol 1,4,5-trisphosphate metabolite inositol monophosphate (IP_1) was quantified in CHO-hUT cells using the IP-One terbium immunoassay. In agreement with previously reported data (43), we observed that hUII induced a time-dependent increase in IP_1 that reached a plateau after 40 min (Fig. 3*A*). Concentration–response curves, constructed after 40 min incubation, revealed that hUT-Pep2 and [Trp^1, Leu^2]hUT-Pep3 induced IP_1 production in CHO cells stably expressing hUT (Fig. 3*B*) but not untransfected CHO-K1 cells after a similar period of incubation (Fig. S3). Compared with hUII (pEC_{50} = 12.54 ± 0.06; E_{max} = 97 ± 1), hUT-Pep2 and [Trp^1, Leu^2]hUT-Pep3 appeared to be less potent ($pEC_{50} < 6$) with reduced efficacy (around 35% for hUT-Pep2 and 60% for [Trp^1, Leu^2]hUT-Pep3 at 10^{-5} M, respectively) at promoting IP_1 production (Fig. 3*B*), acting as weak allosteric agonists.

hUT-derived pepducins trigger $ERK_{1/2}$ phosphorylation through different mechanisms

Kinetic measures, using the CHO-hUT cell line (17), revealed that both hUT-derived pepducins induced $ERK_{1/2}$ phosphorylation. Used at 10^{-6} M, hUT-Pep2 and [Trp^1, Leu^2]hUT-Pep3 exerted their maximal effect at 5 min, similar to hUII (Fig. 3*C*). While a second peak was noticeable for [Trp^1, Leu^2]hUT-Pep3 at 60 min, a similar pattern was not observed for hUT-Pep2 (Fig. 3*C*). We next generated concentration–response curves for each pepducin and hUII (Fig. 3*D*). Compared with hUII (pEC50 = 9.69 ± 0.06 and Emax = 102 ± 2), hUT-Pep2 and [Trp^1, Leu^2]hUT-Pep3 were both less potent (pEC_{50} = 7.26 ± 0.14 and 6.70 ± 0.06, respectively) and less efficacious (E_{max} = 34 ± 2% and 56 ± 2%, respectively) at

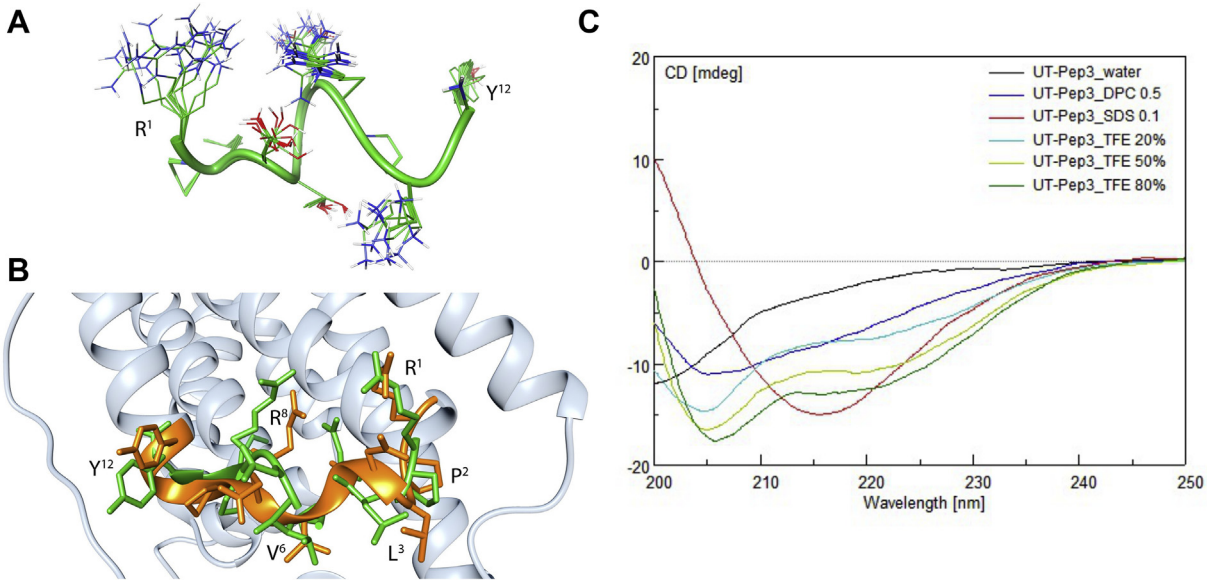

Figure 2. 3D structural data of UT-derived pepducins. *A*, modeled structure of the hUT-Pep2. Ensemble of the ten lowest energy conformers of hUT-Pep2. Structures were superimposed using the backbone heavy atoms. Side chain heavy atoms are shown with different colors (carbon, *green*; nitrogen, *blue*; oxygen, *red*). Many hydrogen atoms and the lipid chains are not shown for clarity. Backbone structure is represented as *green ribbon*. *B*, superposition of hUT-Pep2 structure (representing the NMR lowest energy conformer, *green*) and the second intracellular loop of a hUT model (*orange*). *C*, circular dichroism of [Trp^1, Leu^2]hUT-Pep3 in various solvents.

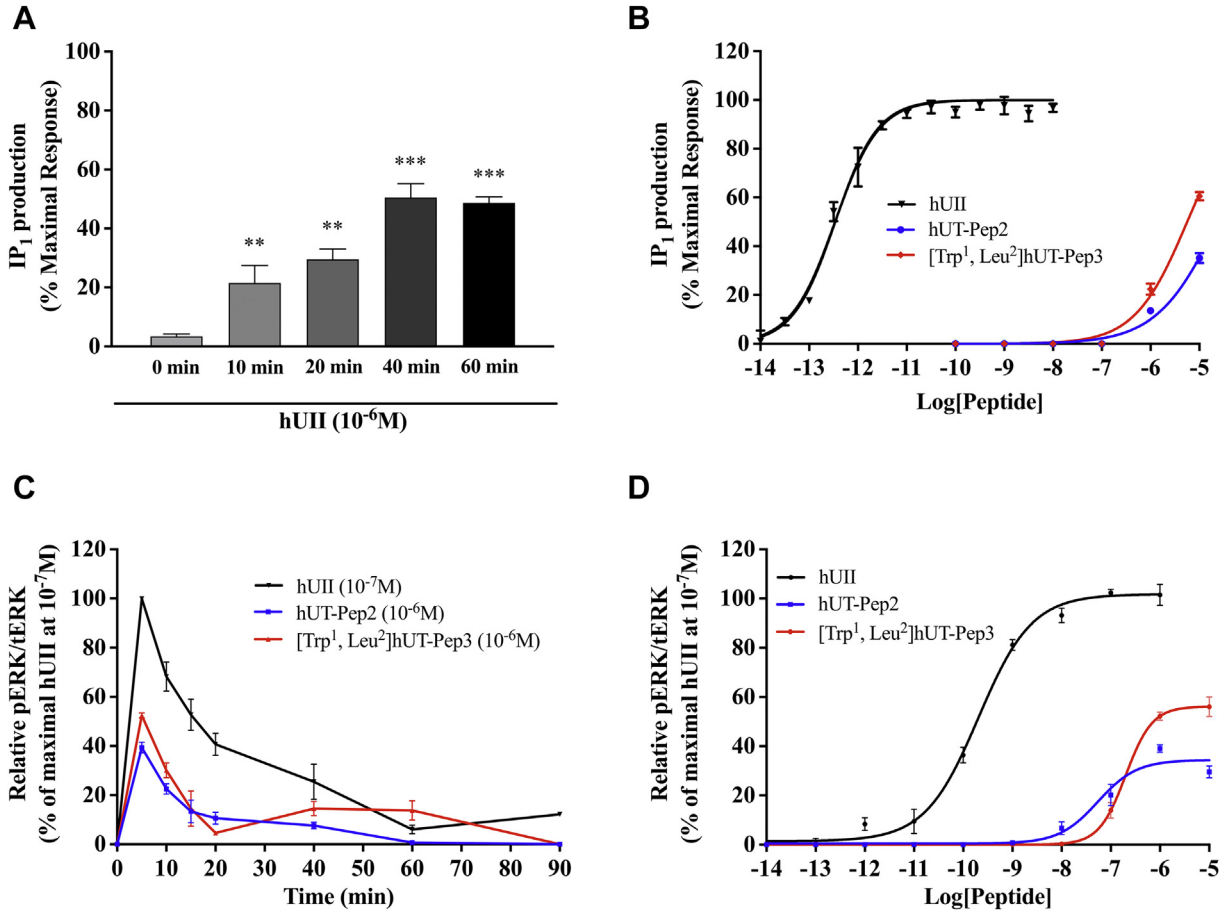

Figure 3. IP$_1$ production (*A* and *B*) and ERK$_{1/2}$ phosphorylation (*C* and *D*) kinetics and concentration dependence following hUT activation. IP$_1$ production was evaluated using the IP-One terbium immunoassay kits while ERK$_{1/2}$ phosphorylation was measured by western blot in CHO-K1 cells stably expressing hUT. The data are normalized to the hUII maximum effect. Each curve represents the mean ± SEM of at least three independent experiments performed in triplicate.

triggering $ERK_{1/2}$ phosphorylation (Fig. 3*D*), behaving as weak partial allosteric agonists.

As shown in Figure 4*A*, in the absence of the receptor, neither hUII nor hUT-derived pepducins were able to induce $ERK_{1/2}$ phosphorylation, therefore demonstrating their specificity for hUT. Following pretreatment of CHO-hUT cells with PTX (a $G_{i/o}$ protein inhibitor), U73122 (a broad range PLC inhibitor), or AG1478 (a specific EGFR inhibitor), $ERK_{1/2}$ phosphorylation was evaluated at 5 min as described above. While PTX and U73122 completely prevented [Trp^1, Leu^2]hUT-Pep3-mediated $ERK_{1/2}$ phosphorylation, hUT-Pep2 action was only partially affected by the PLC inhibitor, further supporting potentially distinct mechanisms of action (Fig. 4, *B* and *C*). Inhibition of EGFR transactivation with AG1478 significantly reduced the ability of both hUT-derived pepducins to induce $ERK_{1/2}$ phosphorylation (Fig. 4*D*).

Further evaluation of their signaling signatures with BRET-based biosensors prompted us to use a HEK 293 cell line stably expressing hUTm since these biosensors were already optimized for a use with a HEK 293 background (44).

Consistent with our previous results, kinetic experiments performed this time in HEK 293 cells stably expressing hUT using western blot, once again revealed a biphasic $ERK_{1/2}$ activation following hUII treatment with a maximum activation after 5 min (Fig. 5*A*). Differences observed in the pattern but not the kinetics of activation of hUII between assays here

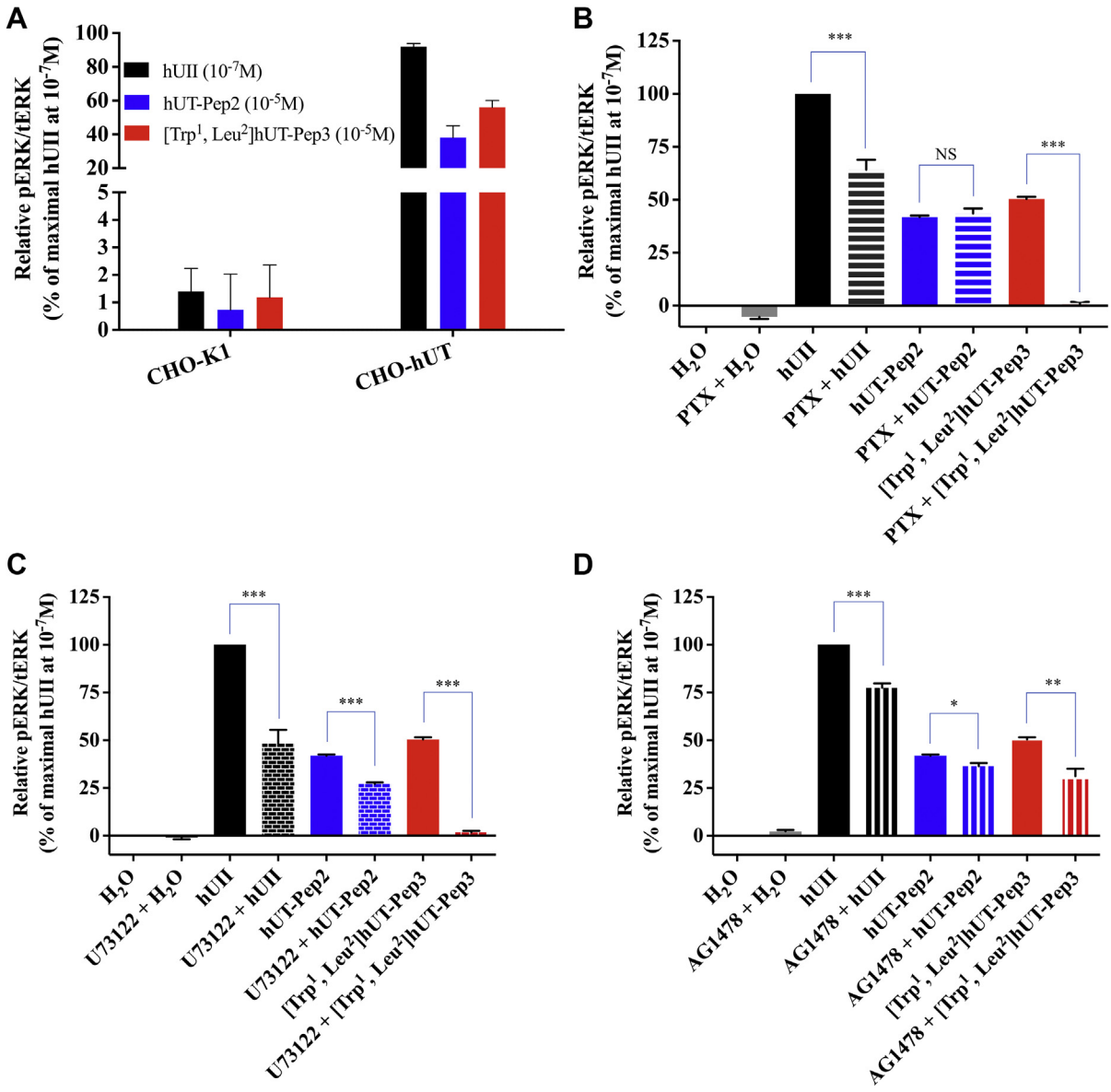

Figure 4. Effect of hUII, hUT-Pep2, and [Trp^1, Leu^2]hUT-Pep3 on $ERK_{1/2}$ phosphorylation in CHO-K1 cells or CHO-K1 cells stably expressing the hUT receptor (CHO-K1-hUT). $ERK_{1/2}$ phosphorylation was measured by western blot. *A*, CHO-K1, which does not express hUT, and CHO-K1-hUT cells were treated for 5 min with hUII (10^{-7} M), hUT-Pep2, or [Trp^1, Leu^2]hUT-Pep3 (10^{-5} M) for 5 min (*B–D*) CHO-K1-hUT cells were treated with hUII (10^{-7} M), hUT-Pep2, or [Trp^1, Leu^2]hUT-Pep3 (10^{-6} M) in the absence or presence of PTX (200 ng/ml, 24 h), U73122 (1 μM, 60 min), or AG1478 (5 μM, 30 min). The data are normalized to the hUII maximum effect at 10^{-7} M and after 5 min incubation. Quantification of $ERK_{1/2}$ phosphorylation level was performed in three independent experiments done in in triplicate (mean ± SEM, n = 3, ***$p < 0.001$, **$p < 0.01$, or *$p < 0.05$, *versus* control).

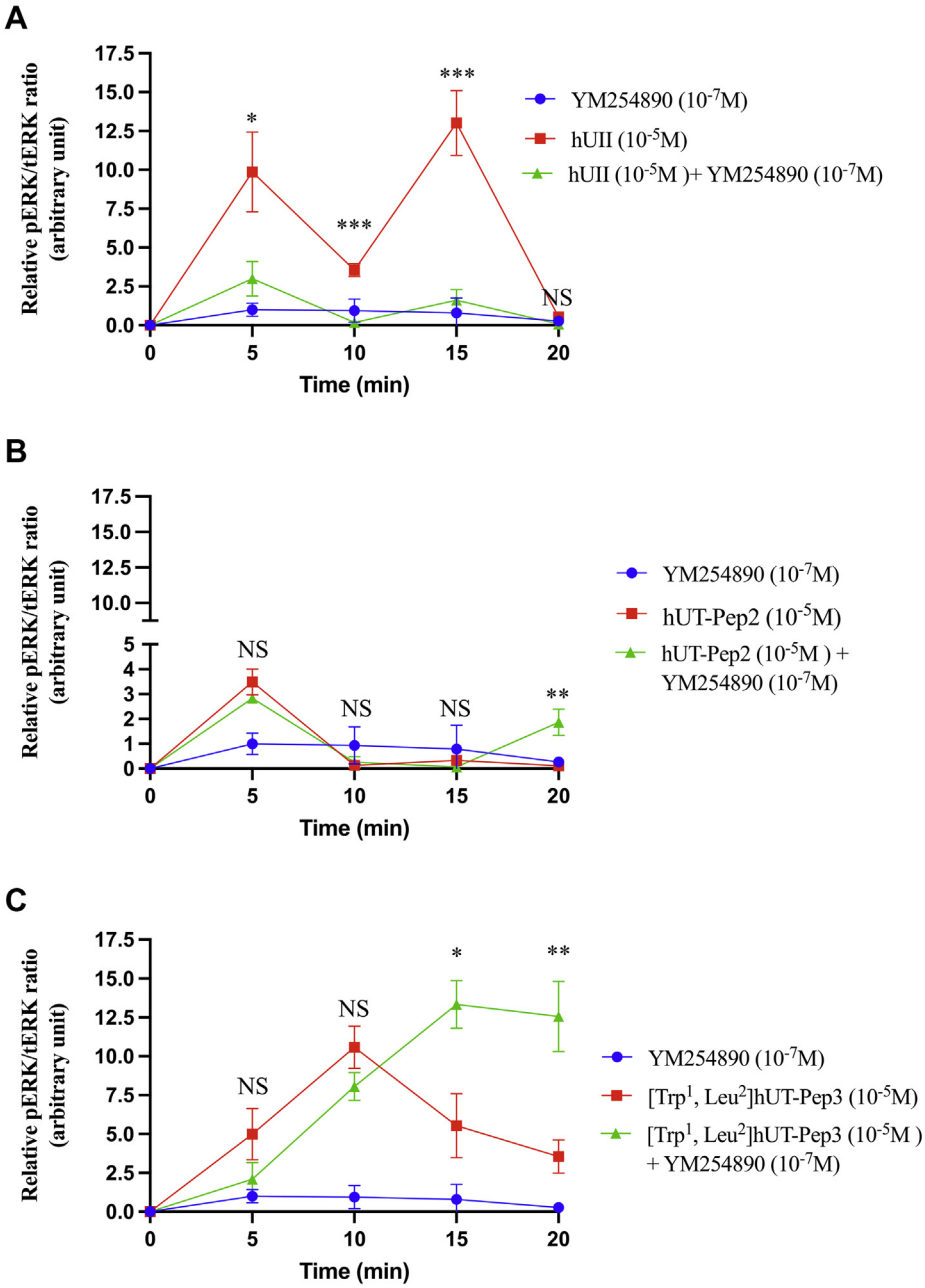

Figure 5. $ERK_{1/2}$ phosphorylation kinetics after hUT receptor activation. hUT-mediated $ERK_{1/2}$ phosphorylation following hUII, hUT-Pep2 or [Trp^1, Leu^2]hUT-Pep3 in the absence or presence of YM254890 was evaluated by western blot. Data are normalized to the hUII maximum effect at each time point. Curves represent mean ± SEM of three independent kinetic experiments performed in triplicate. Statistical comparisons between hUII, hUT-pepducins treated or not with YM254890 were analyzed by the Student's *t* test, and differences were considered significant where $*p < 0.05$, $**p < 0.01$, or $***p < 0.001$.

and those performed in CHO-UT cells are probably attributable to distinct cellular contexts and expression level of hUT. In this assay, hUT-Pep2 (10^{-5} M) also reached its maximal effect after 5 min while [Trp^1, Leu^2]hUT-Pep3 needed 10 min to reach an efficacy similar to that observed with hUII (10^{-7} M) (Fig. 5, *B* and *C*). Pretreatment with YM254890, a selective inhibitor of G_q signaling, almost completely abolished the ability of hUII to increase $ERK_{1/2}$ phosphorylation while having a modest, but significant, inhibitory effect on the actions of hUT-Pep2 (at 5 min, $*p < 0.05$) and [Trp^1, Leu^2]hUT-Pep3 (at 5 and 10 min, $*p < 0.05$) (Fig. 5, *A*–*C*). Similarly, while a small but significant reduction of $ERK_{1/2}$ phosphorylation was observed with [Trp^1, Leu^2]hUT-Pep3 in the presence of YM254890, this activation is maintained and did not decrease over the studied period of time (Fig. 5*C*). Finally, similar to what was observed in CHO-hUT cells using western blotting, the use of a BRET-based ERK1/2 biosensor revealed that hUT-Pep2 and [Trp^1, Leu^2]hUT-Pep3 triggered $ERK_{1/2}$ phosphorylation with lower potency and efficacy than hUII (Fig. S4). Surprisingly, when added together, the combination of both pepducins did not promote a significant phosphorylation of $ERK_{1/2}$ at any given concentration (Fig. S5). By binding to different region of the intracellular surface of hUT at the same time, these derivatives may destabilize the receptor and

prevent its activation. Together, these results support a different mode of action related to the regulation of $ERK_{1/2}$ activity by hUT-Pep2 and [Trp^1, Leu^2]hUT-Pep3.

Signaling signatures of hUT-derived pepducins

We next investigated the propensity of each pepducin to induce G_q, G_{12}, G_i, G_{13} activation or promote conformational changes in β-arrestin 1 and β-arrestin 2 using BRET-based biosensors. As depicted in Figure 6, *A–D* and Table 2, hUT-derived pepducins can promote activation of G_q, G_i, and G_{13} but were almost completely unable to activate G_{12}. Notably, on the one hand, [Trp^1, Leu^2]hUT-Pep3 stimulated G_q activation with a similar potency (pEC_{50} = 8.34 ± 0.33) but a lower efficacy (E_{max} = 29 ± 4%, $^{***}p < 0.001$) than hUII (pEC_{50} = 8.19 ± 0.12; E_{max} = 109 ± 5%) acting as a partial allosteric agonist of this pathway (Fig. 6*A*; Table 2). On the other hand, hUT-Pep2 behaved as a weak partial allosteric agonist (pEC_{50} = 7.31 ±

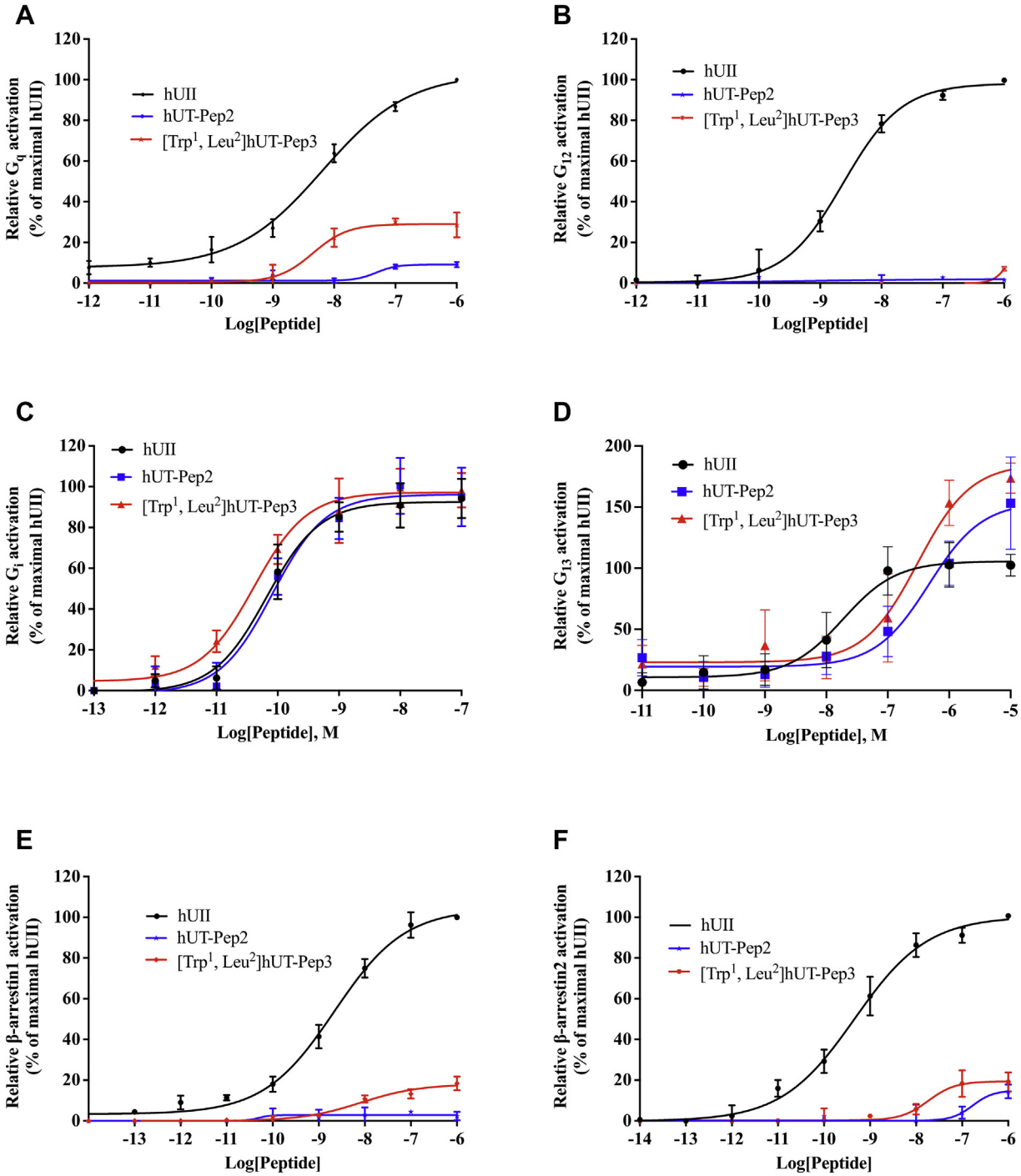

Figure 6. Signaling signature of hUT-pepducins following hUT receptor activation. BRET measurements were performed following hUT stimulation with increasing concentrations of hUII, or hUT-derived pepducins in HEK 293-hUT cells. The data are normalized to maximal hUII responses (10^{-6} M or 10^{-5} M). Each curve represents mean ± SEM of at least three independent concentration-response experiments performed in triplicate.

Table 2
Signaling signatures of hUII and hUT-derived pepducins

Peptides	G_q		G_{12}		G_i		G_{13}		β-arr1		β-arr2	
	pEC_{50} [a]	E_{max} [b]	pEC_{50} [a]	E_{max} [b]	pEC_{50} [a]	E_{max} [b]	pEC_{50} [a]	E_{max} [b]	pEC_{50} [a]	E_{max} [b]	pEC_{50} [a]	E_{max} [b]
hUII	8.19 ± 0.12	109 ± 5	8.62 ± 0.09	98 ± 3	10.18 ± 0.07	93 ± 2	7.73 ± 0.13	106 ± 5	8.66 ± 0.13	104 ± 4	9.33 ± 0.14	100 ± 3
hUT-Pep2	7.31 ± 0.55**	9 ± 1***	-	-	10.09 ± 0.08	96 ± 2	6.33 ± 0.12**	154 ± 10**	-	-	-	15[c]
[Trp^1, Leu^2]hUT-Pep3	8.34 ± 0.33	29 ± 4***	-	5[c]	10.39 ± 0.09	97 ± 2	6.51 ± 0.11**	185 ± 11**	8.08 ± 0.27**	18 ± 2***	7.74 ± 0.32***	19 ± 3***

All values are expressed as mean ± SEM. Statistical analysis was performed using unpaired Student's *t* test.
Statistical analysis was performed using unpaired Student's *t* test, $^{**}p \leq 0.01$, $^{***}p \leq 0.001$, *versus* values obtained for hUII. Each replicate (n = 3–5) was conducted on different cellular passages.
[a] $pEC_{50} = -\log EC_{50}$.
[b] The maximum efficacy is expressed as a percentage of the activation induced by hUII (10^{-6} M).
[c] Maximum efficacy at 10^{-6} M.

0.55) of this pathway reaching approximately 9% of the hUII maximum response (Fig. 6*A*; Table 2). Interestingly, like hUII, both hUT-derived pepducins acted as full agonists for the activation of G_i and G_{13} (Fig. 6, *C* and *D*; Table 2). Notably, while both pepducins promoted G_i in a similar manner than hUII (Fig. 6*C*; Table 2), these derivatives appear to less potent (pEC_{50} = 6.33 ± 0.12 and pEC_{50} = 6.51 ± 0.11, respectively; $^{**}p < 0.01$) but more efficient (E_{max} = 154 ± 10% and E_{max} = 185 ± 11%, respectively; $^{**}p < 0.01$) than hUII (pEC_{50} = 7.73 ± 0.13 and E_{max} = 106 ± 5%) at triggering G_{13} (Fig. 6*D*; Table 2).

We next evaluated the propensity of hUT-derived pepducins to drive conformational changes in β-arrestin 1 and 2. For β-arrestin 1, [Trp^1, Leu^2]hUT-Pep3, which is almost equipotent (pEC_{50} = 8.08 ± 0.27; $^{**}p < 0.01$) compared with hUII (pEC_{50} = 8.66 ± 0.13) but only reached around 18% of its maximum response (Fig. 6*E*; Table 2), acting as a weak partial allosteric agonist for this signaling pathway while hUT-Pep2 appears inactive. For β-arrestin 2, [Trp^1, Leu^2]hUT-Pep3, once again acted as a weak partial allosteric agonist, triggering activation of this pathway with low potency (pEC_{50} = 7.74 ± 0.32; $^{***}p < 0.001$) and efficacy (E_{max} = 19 ± 3; $^{***}p < 0.001$) compared with hUII (pEC_{50} = 9.33 ± 0.14; E_{max} = 100 ± 3%) (Fig. 6*F*; Table 2). hUT-Pep2 behaved as a very weak partial allosteric agonist reaching, at 10^{-6} M, around 15% of the maximal response evoked by hUII. Together, these results demonstrate that both pepducins can trigger hUT activation albeit to different extents.

hUT-derived pepducins promote EGFR transactivation through G_q activation

We next investigated whether hUT stimulation by hUT-Pep2 or [Trp^1, Leu^2]hUT-Pep3 could mediate EGFR transactivation. Untransfected HEK 293 cells and cells overexpressing wild-type hUT were transfected with EGFR-GFP and stimulated with either hUII, hUT-Pep2 or [Trp^1, Leu^2]hUT-Pep3 (10^{-6} M). In the absence of stimulation, EGFR showed a uniform membrane distribution in HEK 293 cells stably transfected or not with hUT (Fig. 7, *A* and *B*). In contrast, treatment with hUII resulted in EGFR internalization as characterized by a marked redistribution into cellular aggregates compared with untreated HEK 293 cells (Fig. 7, *B* and *E*). However, limited EGFR internalization can be observed in untransfected HEK 293 cells, (Fig. S6), perhaps due to the presence of low levels of hUT in this cell line as previously suggested (19). Treatment with hUT-derived pepducins in HEK 293-hUT cells resulted in significant internalization of EGFR-GFP as demonstrated by the punctate distribution of fluorescence (Fig. 7, *H* and *K*). Finally, we observed that pretreatment of the cells with the specific G_q inhibitor YM254890 almost completely abolished hUII- as well as UT-derived pepducin-associated EGFR transactivation (Fig. 7, *F*, *I*, and *L*). Little to no effects of any of the ligands were seen in mock-transfected cells (Fig. 7, *D*, *G*, and *J*). Together, these results revealed that both pepducins can promote EGFR transactivation to different

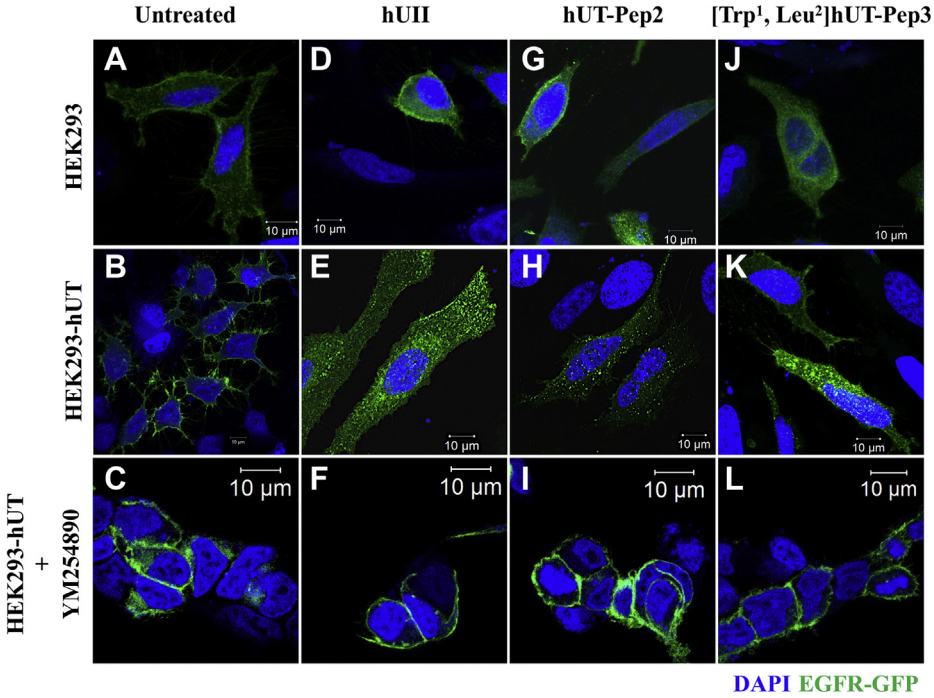

Figure 7. UT-pepducins-mediated transactivation of EGFR following hUT activation. HEK 293 cells stably expressing wild-type hUT (*B*, *E*, *H*, *K*) or not (*A*, *D*, *G*, *J*) and transfected with GFP-EGFR were treated with hUII, hUT-Pep2, or [Trp^1, Leu^2]hUT-Pep3 in the presence (*C*, *F*, *I*, *L*) or not of YM254890. EGFR internalization, following hUT stimulation with various ligands for 30 min, was visualized using confocal microscopy. The images shown are from representative experiments repeated at least three times.

extents and that this activation is abrogated following G_q inhibition.

hUT-Pep2 and [Trp^1, Leu^2]hUT-Pep3 induce rat cardiac neonatal fibroblast proliferation

Several studies have demonstrated the mitogenic properties of UII, URP, and related analogs in various cultured cells (1), including rat fibroblasts (45, 46), and astrocytes (20), as well as HEK 293-hUT cells (43). Here, using HEK 293-hUT cells and two different methods, *i.e.*, MTT assays and flow cytometry, we observed that hUII and [Trp^1, Leu^2]hUT-Pep3 but not hUT-Pep2 were able to induce HEK 293-hUT cell proliferation (Fig. 8, *A* and *C*). Again, in the absence of the receptor, the above described effect was completely abrogated (Fig. 8*B*). Interestingly, using high content imaging, we observed that both hUT-derived pepducins produced a proliferative action in rat neonatal cardiac fibroblasts similar to what was observed with hUII (Fig. 8*D*). These observations showed that hUT-Pep2 and [Trp^1, Leu^2]hUT-Pep3 can act as allosteric agonists promoting cell proliferation and that this action is cell-context-dependent for hUT-Pep2.

hUT-derived pepducins can block hUII- and URP-mediated contraction

Since its discovery, UII and its paralog peptide URP have been considered potent vasoconstrictors (1). As shown in Figure 9*A*, neither of the hUT-derived pepducins was able to stimulate contraction reaching only between 5 and 15% of the force induced by hUII or URP in rat aortic ring preparations (Table 3). Used as potential allosteric modulators, hUT-Pep2 and [Trp^1, Leu^2]hUT-Pep3 suppressed the maximum contractile response to hUII and URP (Fig. 9, *B* and *C*; Table 4). For instance, pretreatment with [Trp^1, Leu^2]hUT-Pep3 at 10^{-6} M, produced significant suppression of maximum contractile responses to hUII (E_{max} = 35 ± 6%; $^{***}p < 0.001$) and URP (E_{max} = 16 ± 2%; $^{***}p < 0.001$) (Table 4). Similarly, hUT-Pep2 at the same concentration promoted a significant but small reduction of the maximum contractile response to hUII (E_{max} = 86 ± 3%; $^{*}p < 0.05$) and URP (E_{max} = 76 ± 8%; $^{**}p < 0.01$). Interestingly, hUT-Pep2 induced a significant rightward shift in the concentration–response curve of hUII but not URP, suggesting a probe-dependent action. These data demonstrate that hUT-Pep2 but most importantly [Trp^1, Leu^2]hUT-Pep3 can negatively modulate hUII- and URP-mediated contraction. Aortic ring contraction mediated by hUT activation generally involves intracellular calcium mobilization following G_q activation (43) and the stimulation of the small GTPase RhoA following $G_{12/13}$ activation (47). Since both pepducins promoted G_q and G_{13} activation but not G_{12} stimulation, we investigated their propensity to block hUII and/or URP-mediated G_{12} activation. As shown in Figure 10, hUT-Pep2 or [Trp^1, Leu^2]hUT-Pep3 pretreatment (10^{-5} M) completely abolished hUII- and URP-associated G_{12} stimulation, which could possibly explain, at least in part, the decrease in efficacy observed in our aortic ring contraction assay.

Discussion

By selectively engaging only a subset of potential intracellular partners, allosteric agonists or biased ligands may offer an

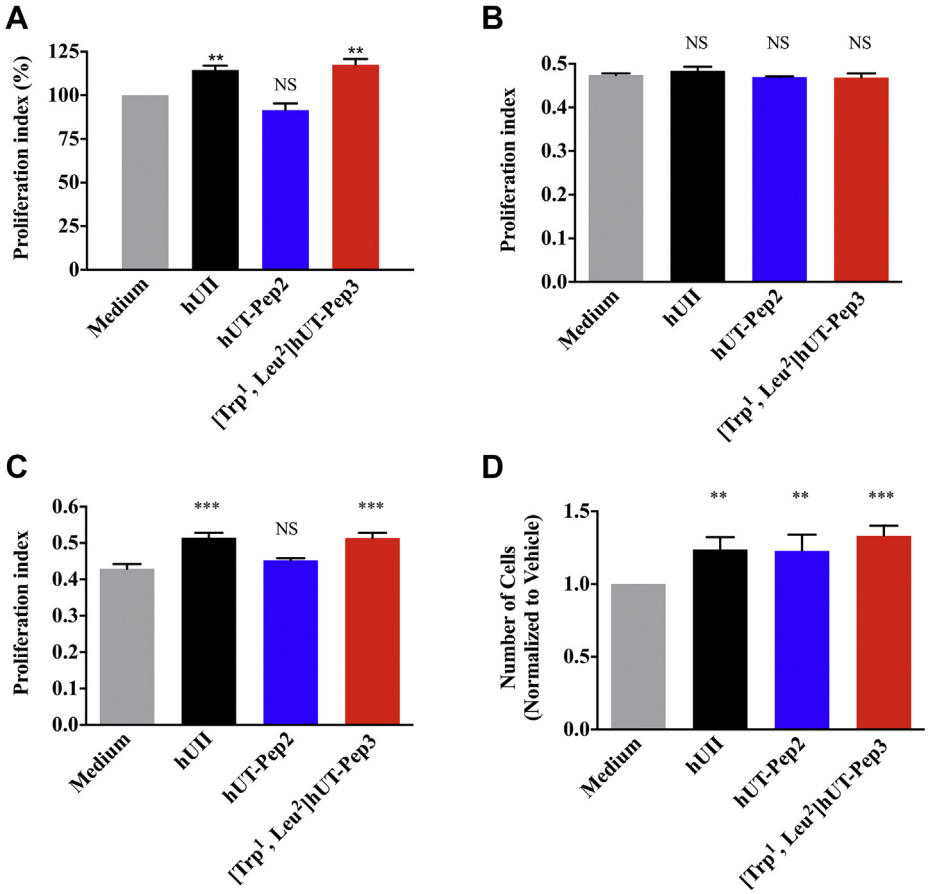

Figure 8. Effects of hUII and UT-derived pepducins on proliferation of hUT receptor-expressing HEK 293 cell and rat neonatal fibroblasts. HEK 293 cells stably expressing hUT were treated with hUII, hUT-Pep2 or [Trp^1, Leu^2]hUT-Pep3 (10^{-6} M) and cell proliferation was evaluated by MTT assay (*A*) or flow cytometry (*C*). HEK 293 cells were treated with hUII, hUT-Pep2 or [Trp^1, Leu^2]hUT-Pep3 (10^{-6} M) and cell proliferation was also evaluated by MTT assay (*B*). *D*, rat neonatal fibroblasts endogenously expressing UT were treated with hUII, hUT-Pep2 or [Trp^1, Leu^2]hUT-Pep3 (10^{-6} M) and proliferation was evaluated with an Opera Phoenix using smooth muscle a-actin as primary antibody and an anti-rabbit Alexa Fluor 488 as secondary antibody. Each bar corresponds to the mean ± SEM obtained from three independent experiments conducted in triplicate.

unparalleled means to understand and control GPCR-mediated signaling (48). Over the years, the pepducin concept has yielded numerous allosteric agonists and antagonists for several GPCRs, some of them reaching clinical trials (49–51). By stabilizing or disrupting molecular interactions that change the energy landscape of a GPCR, pepducins have the potential to affect the conformational ensemble in ways that affect signaling (52). In the present study, we tested the ability of pepducins, derived from the sequence of intracellular loops 2 and 3 of hUT, to act as functionally selective modulators. We first demonstrated that these UT-derived pepducins did not show cytotoxic effects up to 10^{-5} M in concentration. Then, using various BRET-based biosensors, we demonstrated that hUT-Pep2 and [Trp^1, Leu^2]hUT-Pep3 showed a clear bias toward the activation of G_i and G_{13}, compared with G_q or G_{12} activation as well as β-arrestin conformational changes. Most notably, these lipidated peptides, which assumed a three-dimensional structure similar to those adopted in the full-length receptor and did not show any cytotoxic effects, were both able to act as allosteric biased agonists by promoting hUT-related signaling. Compared with hUII, hUT-Pep2 and [Trp^1, Leu^2]hUT-Pep3 were able to stimulate, with lower potency and efficacy compared with hUII, $ERK_{1/2}$ phoshorylation through different mechanisms. hUT-Pep2-induced $ERK_{1/2}$ phosphorylation was partially reduced following treatment of cells with inhibitors of PLC, G_q and EGFR, but unaffected by PTX treatment while the actions of hUII were substantially reduced, or even suppressed, under similar conditions. Therefore, G_i activation does not appear to mediate the effects of hUT-Pep2 on $ERK_{1/2}$ phosphorylation, which likely instead involves G_q, G_{13}, β-arrestin2 as well as EGFR transactivation. However, G_{13}, which is potently stimulated by hUT-Pep2 following hUT activation, can promote $ERK_{1/2}$ activation and inositol production through PLCε, Ras, and RhoA GTPases (53–56). Hence, the weak inhibitory effect of U73122, YM254890, and AG1478 on $ERK_{1/2}$ phosphorylation mediated by hUT-Pep2 suggests that this effect is likely mediated by G_{13}. Conversely, the drastic reduction in [Trp^1, Leu^2]hUT-Pep3-induced $ERK_{1/2}$ phosphorylation following inhibition of G_i or PLC suggested, at first, a possible involvement of G_i and G_q in $ERK_{1/2}$ phosphorylation associated with hUT activation by [Trp^1, Leu^2]hUT-Pep3. As previously reported, inhibition of phospholipase C by U73122 can also block receptor-mediated activation of G_i proteins (57, 58).

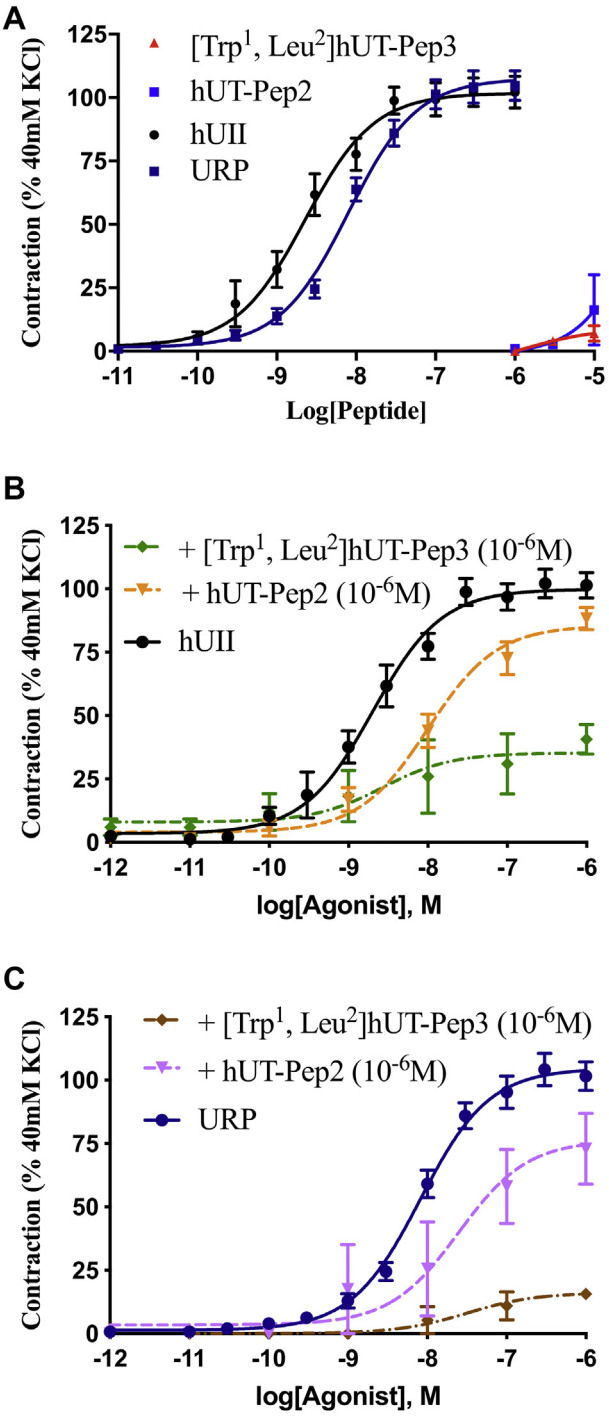

Figure 9. Vasocontractile action of hUT-derived pepducins. *A*, representative concentration–response curves obtained with rat thoracic aorta rings after adding cumulative concentrations of hUII or hUT-derived pepducins. Representative concentration–response curves obtained with rat thoracic aorta rings after adding cumulative concentrations of hUII (*B*) or URP (*C*) following pretreatment with hUT-Pep2 or [Trp^1, Leu^2]hUT-Pep3. Each replicate (n) was conducted on tissue obtained from at least three different animals. Data represent mean ± SEM.

GPCRs are known to activate PLC, either *via* GTP-liganded α subunits of the G_q class of G proteins or by Gβγ dimers liberated from G_i proteins (59). Thus, the complete inhibition of [Trp^1, Leu^2]hUT-Pep3-mediated $ERK_{1/2}$ phosphorylation by either PTX or U73122 suggests a direct connection between

Table 3
Contractile activity of UT-derived pepducins

Compounds	E_{max}[a]	pEC_{50}[b]	n
hUII	102 ± 3	8.64 ± 0.09	22
URP	108 ± 3	8.10 ± 0.06	22
hUT-Pep2	7% @ 10 μM	<5	5
[Trp^1, Leu^2]hUT-Pep3	16% @ 10 μM	<5	5

All values are expressed as mean ± SEM. Each replicate (n) was conducted on tissue obtained from different animals.
[a] Maximum efficacy is expressed as a percentage of the amplitude of contraction induced by depolarization with 40 mM KCl.

the two that might involve Gβγ subunits of G_i. In support of this hypothesis, it was demonstrated that dually coupled GPCRs require cooperation of G_i- and G_q-mediated pathways for efficient stimulation of the $ERK_{1/2}$ cascade (60). However, selective G_q inhibition with YM254890 resulted in only a small, but significant, reduction in the early phase of $ERK_{1/2}$ phosphorylation with a late phase that was both enhanced and sustained (Fig. 5*C*). Discrepancies between this result and the one observed using U73122 (Fig. 4*C*), a broad PLC inhibitor that can also block phospholipase A2 (61), can be explained by the propensity of G_{13} to trigger $ERK_{1/2}$ phosphorylation *via* PLCε and PLA2, both actions being inhibited by U73122 (55, 56). Finally, to explain the effect observed with [Trp^1, Leu^2]hUT-Pep3 following YM254890 treatment, its is possible that a switch from G_q to G_{13} or G_i took place amplifying G_i and/or G_{13}-mediated action. A similar switch has been recently demonstrated to explain the variation in insulin secretion of different incretins (62). Indeed, it was shown that inhibiting the K_{ATP} channel caused a switch from G_s to G_q in an important pathway regulating insulin secretion, which determined the relative insulinotropic effectiveness of incretins (62).

Several studies have suggested that EGFR transactivation plays a critical role in the hypertrophic response evoked by UT in rat cardiomyocytes (63). Interestingly, such activation was prevented by knockdown of β-arrestins (63). However, as demonstrated, the absence of G protein activation prevents β-arrestin signaling (64). To dissect the mechanism of hUII, hUT-Pep2, and [Trp^1, Leu^2]hUT-Pep3-induced EGFR translocation, we transfected HEK 293-hUT cells with GFP-EGFR and monitored internalization by confocal microscopy. When stimulated with hUII or hUT-derived pepducins, GFP-EGFR was redistributed from the plasma membrane into endocytic vesicles. Pretreatment with YM254890 considerably reduced hUII-, hUT-Pep2-and [Trp^1, Leu^2]hUT-Pep3-induced EGFR internalization, indicating a requirement for G_q in their respective responses. Based on previous publications (63), it seems that, at least for hUII, EGFR internalization requires both G_q and β-arrestins. For both pepducins, some punctae can still be seen despite YM254890 pretreatment. Based on their propensity to activate G_{13} and the fact that G_{13} activation can also promote EGFR transactivation as demonstrated for thyrotropin and lysophosphatidic acid receptors (53, 65), we cannot exclude that EGFR transactivation is, at least to some extent, mediated by hUT-pepducin-associated G_{13} stimulation.

Table 4
Effects of pepducins on contractile activities mediated by hUII or URP

Peptide	Aortic ring contraction hUII			Aortic ring contraction URP		
	n	pEC_{50}	E_{max}[a]	n	pEC_{50}	E_{max}[a]
hUII	19	8.69 ± 0.08	100 ± 3			
URP				22	8.09 ± 0.06	105 ± 3
hUT-Pep2	5	8.00 ± 0.11**	86 ± 3*	5	7.60 ± 0.31	76 ± 8**
[Trp[1], Leu[2]]hUT-Pep3	5	8.57 ± 0.63	35 ± 6***	5	8.59 ± 0.12	16 ± 2***

Aortic rings were pretreated with different analogues at a concentration of 10^{-6} M for 30 min prior to hUII or URP treatment. All values are expressed as the mean ± SEM. Statistical analysis was performed using unpaired Student's *t* test, $^{*}p \le 0.05$, $^{**}p \le 0.01$, $^{***}p \le 0.001$, *versus* values obtained for hUII or URP. Each replicate (n) was conducted on tissue obtained from different animals.
[a] Maximum efficacy is expressed as a percentage of the KCl-induced contraction (40 mM) divided by the tissue-response induced by hUII or URP (10^{-6} M).

Following characterization of their signaling signatures in HEK 293-hUT cells, we next investigated the propensity of hUII-, hUT-Pep2, and [Trp[1], Leu[2]]hUT-Pep3 to promote cell proliferation in both heterologous and native cell lines and their effects on aortic ring contraction. As previously reported, downstream signaling linked to the mitogenic HEK 293-hUT responses obtained following UII treatment involved $ERK_{1/2}$ activation and the RhoA/Rho kinase pathway (43). In the present work, we noted that hUII and [Trp[1], Leu[2]]hUT-Pep3, but not hUT-Pep2, were able to stimulate HEK 293-hUT cell proliferation. Since both hUT-derived pepducins were unable to trigger G_{12} activation, differences in the capacity of hUT-Pep2 and [Trp[1], Leu[2]]hUT-Pep3 to exert mitogenic actions could arise, at least in part, from their significantly different efficacy to stimulate $ERK_{1/2}$ phosphorylation, with [Trp[1], Leu[2]] hUT-Pep3 acting as a weak full agonist while hUT-Pep2 behaved as a partial agonist (Fig. S4). As previously demonstrated, hUII can induce development of cardiac remodeling by promoting fibroblast mitogenesis (45). Interestingly, and similar to what was observed with hUII, both hUT-derived pepducins promoted proliferation of rat neonatal cardiac fibroblasts. Such differences in the mitogenic action of hUT-derived pepducins on HEK 293-hUT cells and cardiac fibroblasts might be inferred from their different cellular contexts or differences between receptor isoforms. Indeed, it is now widely accepted that GPCRs can adopt multiple conformations upon ligand binding and that structurally distinct ligands can stabilize functionally distinct conformations (66). However, parameters that influence the mechanisms and the timescales by which ligands induce/stabilize specific conformations will most likely differ depending on cellular context because of disparities in associated signaling proteins and the composition of the lipid bilayer (67, 68). Also, despite a similar tissue distribution, structural differences between rat and human UT isoforms (only 75% sequence similarity while rat and mouse UT share more than 95% homology) as well as distinct patterns of putative phosphorylation and palmitoylation sites probably lead to differences in signaling, internalization, and desensitization patterns (2). Such differences could therefore also explain the distinct biological activities observed with hUT-Pep2 in HEK 293-hUT cells and rat neonatal fibroblasts. Finally, both endogenous ligands of the urotensinergic system are known as potent vasoconstrictors (1). In the present study, neither hUT-derived pepducin exhibited significant contractile action in rat aortic ring preparations. Since aortic ring contraction is in part mediated by intracellular calcium mobilization following activation of G_q (22, 23, 43) and by the stimulation of the small GTPase RhoA following G_{12}/G_{13} activation (47), the weak contractile potency of hUT-Pep2 and [Trp[1], Leu[2]]hUT-Pep3 could be explained by their inability to trigger sustained G_{12} and/or G_q activation. This is perhaps not surprising as receptor expression is low. We therefore hypothesized that these pepducins, which mostly act as weak

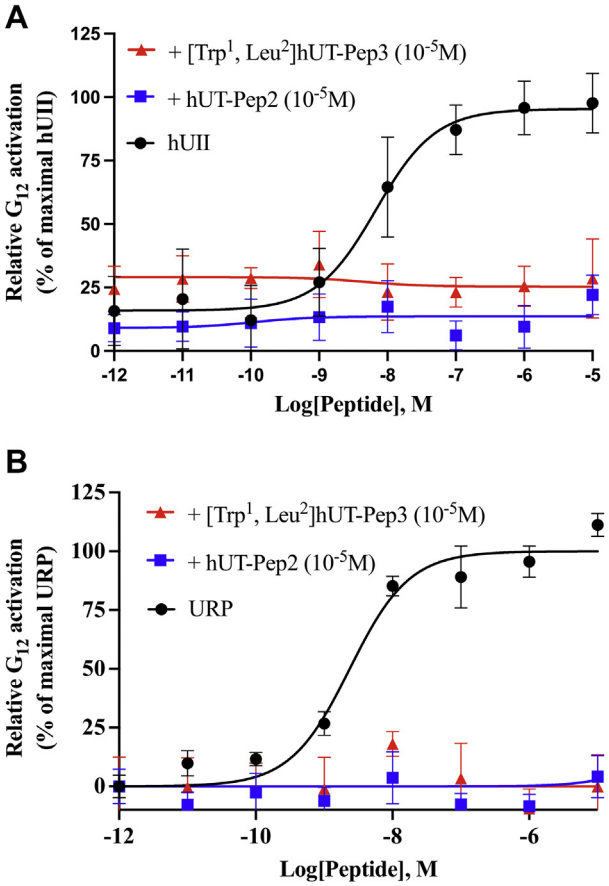

Figure 10. Effect of hUT-pepducins on hUT-mediated G_{12} activation. Representative concentration–response curves obtained after cumulative additions of hUII (*A*) or URP (*B*) following pretreatment with hUT-Pep2 or [Trp[1], Leu[2]]hUT-Pep3 at 10^{-5} M for 15 min. The data are normalized to maximal hUII or URP responses (10^{-5} M). Each curve represents mean ± SEM of at least three independent concentration–response experiments performed in triplicate.

agonists in receptor overexpressing cells, could behave as modulators of hUII and URP in an endogenous context. We therefore tested whether agonist-stimulated aortic ring contraction was inhibited by either hUT-Pep2 and/or [Trp^1, Leu^2]hUT-Pep3. Interestingly, both pepducins were able to reduce hUII- and URP-mediated contraction to different extents, an effect that could be attributed to their ability to antagonize hUII- and URP-mediated G_{12} activation. Understanding how hUT-pepducins exert their action at the molecular level will need further study. However, and as proposed for other reported pepducins, pepducins acting as negative modulators, could (1) compete with their homologous peptide segments, buffering/hindering the interaction of signaling partners and/or components of signaling cascade or (2) interact with complementary regions of the peptide segment, *i.e.* intracellular loops or transmembrane domains, therefore destabilizing (antagonism) receptor conformations and dynamics ultimately modulating associated signaling (33).

Conclusions

Taken together, our results demonstrate that hUT-Pep2 and [Trp^1, Leu^2]hUT-Pep3, derived from the intracellular loops 2 and 3, respectively, of hUT can act as biased allosteric agonists/antagonists, engaging/preventing different signaling pathways following UT activation. Given that pepducins are believed to act intracellularly by binding directly to targeted GPCRs on the inner face of the membrane (52, 69), it is not surprising to observe that different subsets of downstream effectors than those promoted by the binding of hUII are engaged. Interestingly, while hUT-Pep2 and [Trp^1, Leu^2]hUT-Pep3 can trigger cell proliferation, this effect appears to be dependent on cellular context. The precise mechanisms of action by which hUT-derived pepducins can promote G_q/G_i activation, EGFR transactivation, and fibroblast proliferation are still unknown and will need further investigation. These new molecular tools could represent innovative UT-targeted modulators with unique pharmacological profiles.

Experimental procedures

Cell lines and reagents

HEK 293 cells were purchased from ATCC while the stably transfected HEK 293-hUT cell line was generated in our laboratory (23). Cell culture reagents were obtained from Invitrogen while antibodies used to evaluate $ERK_{1/2}$ phosphorylation, *i.e.*, a rabbit polyclonal antibody against phospho-p44/42 MAPK and an anti-total MAP kinase antibody, were purchased from Cell Signaling Technology. α-Actin antibody was obtained from Abcam. The IP-One ELISA assay kit from CisBio Bioassays. The fluorenylmethyloxycarbamate-(Fmoc-) protected amino-acids, Rink amide AM resin (with Nle), N,N′-diisopropylcarbodiimide (DIC), and ethyl cyanohydroxyiminoacetate (Oxyma) were purchased from ChemImpex. Trifluoroacetic acid (TFA), methanol (MeOH), acetonitrile (ACN), diethyl ether, N,N-dimethylformamide (DMF), piperidine, dichloromethane (DCM), and cell mask were obtained from Fisher Scientific. YM254890 was purchased from Cedarlane. All other chemicals, including 99.9% ^2H_2O, were from Sigma-Aldrich. 98% DPC-d_{38} was obtained from Cambridge Isotope Laboratories, Inc, and [(2,2,3,3-tetradeuterio)-3-(trimethylsilanyl)]propionic acid (TSP) from MSD Isotopes.

Synthesis of hUT-derived pepducins

hUT-derived pepducins were synthesized manually using a standard solid-phase peptide synthesis approach with Fmoc chemistry. Coupling efficiency was monitored with the qualitative ninhydrin test and a 3-equivalent excess of the protected amino acids, based on the original substitution of the resin (0.50 mmol g^{-1}), was used in most cases. Coupling of protected amino acids was mediated by DIC (1.5 eq) and Oxyma (1.5 eq) in DCM for 1 h. Fmoc removal was achieved with 20% piperidine in DMF for 20 min. All peptides were cleaved from the resin support with simultaneous side chain deprotection by treatment with TFA containing 1,2-ethanedithiol (2.5%), water (2.5%) and triisopropylsilane (1%) for 1.5 h at room temperature. The diethyl ether-precipitated crude peptides were solubilized in 70% acetic acid (1 mg/ml) and lyophilized prior to purification. Each crude peptide was purified using a preparative reversed-phase HPLC (RP-HPLC) protocol using a linear gradient from eluent A to B with 1% B per 2 min increments (Eluent A = H_2O, 0.1% TFA, Eluent B = 80% CH_3CN/20% H_2O, 0.1% TFA). Homogeneity of purified fractions was assessed by RP-HPLC (eluent system: A = H_2O (0.1% TFA) and B = 100% CH_3CN with a gradient slope of 1% B/min, at flow rate of 1 ml/min on a Vydac C_{18} column) and MALDI-TOF mass spectrometry in linear mode using α-cyanohydroxycinnamic acid as matrix. Fractions presenting both the correct mass, as evaluated by MALDI-TOF mass spectrometry, and a purity higher than 98%, as confirmed by analytical RP-HPLC, were pooled, lyophilized, and stored as a powder until use (Table 1). The synthesis of human urotensin II (hUII) was carried out as reported earlier (17, 18)

Nuclear magnetic resonance

Samples for NMR spectroscopy were prepared by dissolving the appropriate amount of peptide in 0.54 ml of ^1H_2O (pH 5.5), 0.06 ml of ^2H_2O to obtain a final DPC-d_{38} concentration of 2 mM and 200 mM. NMR spectra were recorded on a Varian INOVA 700 MHz spectrometer equipped with a z-gradient 5 mm triple-resonance probe head. All spectra were recorded at a temperature of 25 °C and were calibrated relative to TSP (0.00 ppm) as internal standard. One-dimensional (1D) NMR spectra were recorded in the Fourier mode with quadrature detection. The water signal was suppressed by gradient echo (70). Two dimensional (2D) DQF-COSY (71, 72), TOCSY (73), and NOESY (74) spectra were recorded in the phase-sensitive mode as described (75). Data block sizes were 2048 addresses in t_2 and 512 equidistant t_1 values. Before Fourier transformation, the time domain data matrices were multiplied by shifted sin^2 functions in both dimensions. A mixing time of 70 ms was used for the TOCSY experiments. NOESY experiments were run with mixing time of 100 ms. The qualitative and quantitative analyses of DQF-COSY, TOCSY, and NOESY

spectra were obtained using the interactive program package XEASY (76). Complete ^{1}H NMR chemical shift assignments were effectively achieved for hUT-Pep2 and [Trp^{1}, Leu^{2}]hUT-Pep3 according to the Wüthrich procedure (77) *via* the usual systematic application of DQF-COSY, TOCSY, and NOESY experiments with the support of the XEASY software package (Tables S1 and S3). $^{3}J_{\alpha N}$ coupling constants were measured by 1D proton and DQF-COSY spectra. Temperature coefficients of the amide proton chemical shifts were calculated from 1D ^{1}H NMR and 2D TOCSY experiments performed at different temperatures in the range 25–40 °C by means of linear regression. Observed NOEs are reported in Tables S2 and S4.

Structure determination

The NOE-based distance restraints were obtained from NOESY spectrum of hUT-Pep2 collected with a 100 ms mixing time. The NOE cross-peaks were integrated with the XEASY program and were converted into upper distance bounds using the CALIBA program incorporated into the DYANA program package (Table S2) (78). Since palmitate moiety is mostly unstructured, it was replaced by an acetyl group in the model used for structure calculation. An error-tolerant target function (tf-type=3) was used to account for the peptide intrinsic flexibility. From the produced 100 conformations, ten structures were chosen, whose interproton distances best fitted NOE derived distances, and then refined through successive steps of restrained and unrestrained energy minimization using the Discover algorithm (Accelrys) and the consistent valence force field (CVFF) (79). Molecular graphics images were produced using the UCSF Chimera package (80).

Circular dichroism

Circular dichroism (CD) analyses were performed in a JASCO J-815 (JAPAN Spectroscopy & Chromatography Technology) spectropolarimeter coupled to a temperature controller Peltier. Samples were dissolved at 0.2 mg mL^{-1} in either water, 0.5 mg mL^{-1} DPC (dodecylphophocholine), 0.1 mg mL^{-1} SDS (sodium dodecyl sulfate), or TFE (2,2,2-trifluoroethanol) aqueous solutions at concentrations of 20%, 50%, and 80%. The CD spectra were recorded in the measured range of 200–250 nm using a scan speed of 50 nm min^{-1}, and the baseline was corrected by subtraction of the solvent spectrum. The temperature was set to 20 °C.

Cell culture

CHO-K1, HEK 293, as well as CHO and HEK 293 cells stably transfected with the human urotensin II receptor isoform (CHO-hUT and HEK 293-hUT, respectively) were cultured in Dulbecco's Modified Eagle's Medium (DMEM) supplemented with 10% of heat-inactivated foetal bovine serum (FBS), 100 units mL^{-1} of penicillin, 100 μg mL^{-1} of streptomycin, and 2 mM of L-glutamine. Cells were maintained as a monolayer at 37 °C in a humidified atmosphere of 5% CO_2 and 95% air and passaged by trypsinization once cells reached 70–80% confluence.

Cell viability

HEK 293 cells were seeded at a density of 2 × 10^{4} cells/well in 96 well-plates and cultured at 37 °C for 24 h. Cells were then incubated in serum-free media with hUT-derived pepducins at various concentrations (10^{-8} M–10^{-4} M). Viability was assessed with an MTS kit (CellTiter 96 AQ$_{ueous}$, Promega) and a microplate reader (MTX^{TC} Revelation, Dynex Tech) in order to determine the optical density related to the conversion of MTS into purple-colored water-soluble formazan. Positive control (cells treated with 10% DMSO) and negative control (nontreated cells) were included in each experiment. Results were expressed as the percentage of control (nontreated cells). The presence of lactate dehydrogenase (LDH), released in the culture medium from dead cells, was also determined using a commercial LDH kit (BioVision). Positive control (cells treated with lysis buffer) and negative control (nontreated cells) were included in each experiment. Results were expressed as the percentage of the maximum LDH release following cell lysis.

Western blotting

CHO cells stably expressing hUT (CHO-hUT; gift from Drs H. Vaudry et C. Dubessy, University of Rouen, France) were grown in 12-well plates to 70–80% confluence and starved for 6 h in a serum-free medium. For kinetic experiments, cells were incubated for different time periods (0, 5, 10, 15, 20, 40, 60, and 90 min) with a fixed concentration of hUT-Pep2 or [Trp^{1}, Leu^{2}]hUT-Pep3 (10^{-6} M), hUII (10^{-7} M), or PBS alone (basal control condition). To establish concentration–response curves, cells, seeded as previously described, were stimulated for 5 min with various concentrations of hUII or hUT-derived pepducins (10^{-14}–10^{-5} M). When applicable, CHO-hUT cells were incubated with either pertussis toxin (PTX, 200 ng mL^{-1}) for 24 h, a specific EGFR inhibitor (AG1478; 5 μM) for 30 min, or a PLC inhibitor (U73122; 1 μM) for 60 min prior their stimulation with hUII (10^{-7} M) or hUT-derived pepducins (10^{-6} M). Similar kinetic experiments were also performed in HEK 293-hUT cells in the presence or absence of a specific G_q inhibitor. Briefly, HEK 293-hUT cells, grown in 12-well plates to 70–80% confluence, were starved for 6 h in a serum-free medium. Cells were treated with YM254890 (100 nM) for 1 h and then incubated for different time periods (0, 5, 10, 15, and 20 min) with a fixed concentration of hUII, hUT-Pep2 or [Trp^{1}, Leu^{2}]hUT-Pep3 (10^{-5} M). Cells were then rinsed twice with ice-cold PBS and homogenized in 0.5 ml of lysis buffer (20 mM Tris, 150 mM NaCl, 1 mM EDTA, 1 mM EGTA, 1% Triton X-100, 2.5 mM sodium pyrophosphate, 1 mM β-glycerolphosphate, 1 mM Na_3VO_4, 1 μg mL^{-1} leupeptin, 1 mM PMSF, 1 mM DTT) at 4 °C. Insoluble material was removed by centrifugation at 12,000 rpm for 30 min. The extract was treated with Laemmli sample buffer and heated for 5 min at 95 °C. Aliquots were assayed for protein concentration (BioRad) and an equal amount of total protein was subjected to 12% SDS–PAGE, followed by transfer to a nitrocellulose membrane. The membrane was blocked and then probed with primary antibody (phospho-p44/42 MAPK) at the optimal dilution (1/2000) with

gentle agitation overnight at 4 °C. After washing with TTBS, membranes were then incubated with secondary antibody, conjugated with horseradish peroxidase (anti-rabbit HRP) diluted in TBST containing 5% skim milk (w/v) for 1 h at room temperature. Immunoreactive species were visualized by enhanced chemiluminescence using X-ray film and Thermo Scientific SuperSignal chemiluminescent substrates according to the manufacturer's instructions. Films were digitized and the intensity of the immunoreactive bands determined using Quantity One software from Bio-Rad. To confirm equal protein loading in individual lanes, the membrane was stripped and reprobed with antibody against total $ERK_{1/2}$ (diluted 1:5000).

Bioluminescence resonance energy transfer experiments

HEK 293-hUT cells were grown in DMEM culture media supplemented with 10% foetal bovine serum, HEPES, sodium pyruvate, and G418 (200 μg mL^{-1}). Passages were performed when cells reached 80% of confluency. Cells were initially plated in 96-well plates at a density of 10,000 cells/well. The following day, the medium is replaced with DMEM culture media supplemented with 2.5% foetal bovine serum (FBS), and 12 h later, cells were transiently transfected with 25 ng/well of a Gq-polycistronic, 25 ng/well of a G_{12}-polycistronic BRET sensor, 25 ng/well of a G_{13}-polycistronic BRET sensor, 2.5 ng/well pIRESB RLucII-ERK-NLS-GFP BRET sensor, 2.5 ng β-arrestin 1-polycistronic BRET sensor, or 2.5 ng β-arrestin 2-polycistronic BRET sensor using Lipofectamine2000 at a ratio of 3:1 (Lipofectamine/plasmid DNA) in serum-free Opti-MEM (44, 81). Sixteen hours posttransfection, medium was replaced with DMEM supplemented with 10% FBS, HEPES, sodium pyruvate and G418 (200 μg mL^{-1}) and cell growth was resumed for another 16 h. Cells were washed with 150 μl PBS solution supplemented with 0.1% of glucose and then incubated with 80 μl of this solution for 2 h. Then, to evaluate G_q and G_{12} activation, 10 μl of a 1/20 dilution (diluted before use) of coelenterazine 400A (stock at 1 mM in ethanol) in Kreb's buffer and 10 μl of the 10× appropriate concentration of peptide were added, and the luminescence was evaluated with an Infinite M1000 PRO. For β-arrestin 1 and 2 pathways, hUII, hUT-Pep2, or [Trp^1, Leu^2]hUT-Pep3 at various concentrations was first incubated for 15 min at RT prior adding coelenterazine (10 μl of a 1/20 dilution). To test the antagonist behavior of hUT-Pep2 or [Trp^1, Leu^2]hUT-Pep3, cells were preincubated with one pepducin at 10^{-5} M for 15 min to reach equilibrium, prior to the addition of increasing concentrations of hUII or URP (10^{-12} M–10^{-5} M). Readings were performed after 5 min using an Infinite M1000 PRO. Filters were set at 410 nm and 515 nm for detecting the *Renilla* luciferase II (RlucII, donor) and green fluorescent protein 10 (GFP10, acceptor) light emission, respectively. BRET ratio was determined by calculating the ratio of the light emitted by GFP10 over the light emitted by the RlucII. BRET signals were normalized to that of hUII (10^{-6} M).

IP_1 assay

This assay, performed with the IP-One terbium immunoassay kits from Cisbio, was used according to the manufacturer recommendation and as previously described (43). Briefly, CHO-hUT cells were grown in 10-cm dishes for 24 h. The cells were then starved without serum. The next day, cells were washed once with PBS and collected in PBS containing 20 mM EDTA. For the assay, 80,000 cells per well (96-well plate) were used. Cells were treated for various time (10, 20, 40, and 60 min) at 37 °C with hUII or treated with increasing concentrations of hUII, hUT-Pep2 or [Trp^1, Leu^2]hUT-Pep3 for 40 min at 37 °C. IP_1-d_2 and anti-IP_1-cryptate were added for an additional 2 h at room temperature. Plates were read on a Flexstation 3 microplate reader.

EGFR transactivation

HEK 293 and HEK 293-hUT cells, transiently transfected with cDNA encoding fluorescently labeled EGFR (EGFR-GFP) (2 μg), were plated onto 35-mm glass-bottomed culture dishes (MatTek Corp). Following stimulation, cells were washed once with PBS and fixed in 4% paraformaldehyde for 15 min. To study the involvement of G_q in EGFR internalization, cells were treated with YM254890 (100 nM) for 1h prior peptide treatments. EGFR internalization following hUII, hUT-Pep2, or [Trp^1, Leu^2]hUT-Pep3 stimulation (10^{-6} M) was visualized by green fluorescence using a single sequential line of excitation on a Zeiss LSM 780 Axio Observer Z1 (Carl Zeiss Microimaging). EGFR-GFP internalization was visualized using a combination of excitation (488 nm) and emission filters (499 and 520 nm).

Proliferation assays

HEK 293-hUT cell proliferation was evaluated by flow cytometry using propidium iodide DNA staining. Cells, grown in 6-well plates to 80% confluency, were starved for 6 h in a serum-free medium and then treated with hUII, hUT-Pep2, or [Trp^1, Leu^2]hUT-Pep3 (10^{-6} M) for 30 min at RT. Next, cells were detached, fixed with cold 70% ethanol, and then stored at −20 °C for at least 2 h. Cells were centrifuged at 200 rpm for 10 min at 4 °C and washed at least once with cold PBS. Cells were then resuspended in Triton X-100 (0.1%) supplemented with propidium iodide (500 μg mL^{-1}), and 200 μg mL^{-1} of DNAse-free RNAse A in PBS. Data, expressed as the mean ± SEM of at least three independent experiments, were acquired on a FACScan (BD Biosciences), and results were analyzed with the FlowJo v10 software. The proliferation index is defined as the total number of divisions divided by the number of cells that went into division.

Rat aortic ring contraction

Adult male Sprague-Dawley rats (Charles-River) weighing 250–300 g were housed in cages under controlled illumination (12:12 h light–dark cycle), humidity, and temperature (21–23 °C) and had free access to tap water and rat chow. All experimental procedures were performed in accordance with regulations and ethical guidelines from the Canadian Council for the Care of Laboratory Animals and received approvals of the institutional animal care and use committee of the *Institut National de la Recherche Scientifique—Centre*

Armand-Frappier Santé Biotechnologie. As previously described (17, 18), the thoracic aorta was cleared of surrounding tissue and then excised from the aortic arch to the diaphragm. Conjunctive tissues were next removed from the thoracic aorta and the vessels were divided into five rings of 4 mm. The endothelium of each aortic ring was removed by gently rubbing the vessel intimal surface. Aortic rings were then placed in a 5 ml organ bath filled with oxygenated normal Krebs–Henseleit buffer. Eighty microliters of a 2.5 M potassium chloride solution (40 mM final concentration) was used to evaluate maximal contractile responses of each vessel. In one bath, hUII (10^{-6} M) was applied as a control, and the tissue response was expressed as the ratio with the KCl-induced contraction. Cumulative concentration–response curves to synthetic peptides were obtained by increasing the concentration of each peptide in the remaining organ chambers (10^{-11}–10^{-5} M). The amplitude of the contraction induced by each concentration of peptide was expressed as a percentage of the KCl-induced contraction divided by the tissue response induced by hUII. Antagonist activity of hUT-derived pepducins was evaluated by exposing first the aortic ring to hUT-Pep2, or [Trp^1, Leu^2]hUT-Pep3 (10^{-5} M) for 30 min, to ensure that the peptide reached equilibrium and that no agonist effect is observed, and then adding cumulative concentration of hUII or URP (10^{-12}–10^{-6} M). The median effective concentrations (EC_{50}) are expressed as the mean ± SEM, and the *n* values, representing the total number of animals from which the vessels were isolated, varied from 5 to 8 animals.

Rat cardiac neonatal fibroblast proliferation

Neonatal cardiac rat fibroblasts, endogenously expressing UT (82), were obtained from 1–3-day-old Sprague-Dawley pups as previously reported (83). Briefly, hearts obtained from neonatal rats were enzyme-digested and after centrifugation, cells were preplated to separate cardiomyocytes from fibroblasts. As reported, the adherent nonmyocyte fractions correspond predominantly to fibroblasts while the supernatants largely contain the cardiomyocytes. After several washes, attached fibroblasts were trypsinized and then cultured at 37 °C in 96-well plate (6000 cells per well) in low glucose-DMEM supplemented with 7% FBS, 100 units/ml of penicillin, and 100 μg/ml of streptomycin. After 48 h, cells were washed twice with low glucose-DMEM, and starved for 12 h in this medium. Cells were then treated for 24 h with hUII, hUT-Pep2, or [Trp^1, Leu^2]hUT-Pep3 at a concentration of 10^{-6} M. Prior to staining, cells were fixed with 4% paraformaldehyde for 15 min at RT, permeabilized with 0.2% Triton X-100 in PBS for 5 min, and then blocked with 10% horse serum in PBS for 1 h at RT. Cells are incubated with primary anti-smooth muscle α-actin antibody (1/500) in 10% horse serum/PBS overnight at 4 °C and later with secondary anti-rabbit Alexa Fluor 488 (1/1000) for 1 h at RT. Cell staining was performed using cell mask (1 μg mL^{-1}) in PBS for 30 min at room temperature and with Hoechst dye in PBS (1 μg/ml) for 10 min. Analysis was performed on an Opera Phoenix High Content Imaging System with a 20× water objective.

Statistical analysis

All experiments were performed at least in triplicate. Data, expressed as mean ± SEM, were analyzed with the Prism Software (Graphpad Software). Sigmoidal concentration–response curves fitted with variable slope were used to determine EC_{50}. Statistical comparisons were analyzed by the Student's *t* test, and differences were considered significant where $^{*}p < 0.05$, $^{**}p < 0.01$, or $^{***}p < 0.001$.

Data availability

The ensemble of hUT-Pep2 NMR-derived structures has been deposited in the Protein Data Bank (PDB) with the following code: 6HVK. All remaining data are contained within the article.

Supporting information—This article contains supporting information (84).

Acknowledgements—We thank the Canadian Institutes of Health Research (CIHR), the Natural Sciences and Engineering Research Council of Canada (NSERC) and Heart and Stroke Canada for funding.

Author contributions—H. N., T. A. H., R. D. M., J. C. C. D., M. L., A. C., B. G. A., A. F., T. E. H., and D. C. conceptualization; H. N., R. D. M., J. C. C. D., A. C., T. E. H., and D. C. data curation; H. N., T. A. H., R. D. M., J. C. C. D., E. B., M. L., A. C., B. G. A., J. C. T., T. E. H., and D. C. formal analysis; A. F. and D. C. funding acquisition; H. N., T. A. H., R. D. M., J. C. C. D., E. B., A. C., B. G. A., J. C. T., and T. E. H. investigation; H. N., T. A. H., R. D. M., J. C. C. D., E. B., M. L., A. C., J. C. T., A. F., T. E. H., and D. C. methodology; Supervision, J. C. T., T. E. H., and D. C.; M. L., E. N., A. C., A. F., T. E. H., and D. C. writing–original draft; H. N., R. D. M., J. C. C. D., E. N., A. C., B. G. A., J. C. T., A. F., T. E. H., and D. C. writing–review and editing.

Funding and additional information—This work was supported by a grant from the Heart and Stroke Foundation of Canada (G-15-0008938) and the Canadian Institutes of Health Research (PJT-159687) to T. E. H. and J. C. T, a grant from the Canadian Institutes of Health Research to D. C. (MOP-142184) and a grant from the Natural Sciences and Engineering Research Council of Canada (RGPIN-2015-04848) to D. C. R. D. M. was supported by studentships from the McGill-CIHR Drug Development Training Program and the McGill Faculty of Medicine and Health Sciences. H. N. was supported by a fellowship from the Fonds de Recherche en Santé du Québec. J. C. C. D was supported by the Barbara & Edward Victor award granted by McGill Faculty of Medicine. T. E. H. holds the Canadian Pacific Chair in Biotechnology.

Conflict of interest—The authors declare that they have no conflicts of interest with the contents of this article.

Abbreviations—The abbreviations used are: 7TMR, 7-transmembrane receptor; BOP, (benzotriazol-1-yloxy)tris(dimethylamino) phosphonium hexafluorophosphate; BRET, bioluminescence resonance energy transfer; CHO cells, Chinese hamster ovary cells; DCM, dichloromethane; DIEA, N,N-diisopropylethylamine; DMF,

dimethylformamide; DPC, dodecylphosphocholine; DQF-COSY, double-quantum filtered correlated spectroscopy; Fmoc, fluorenylmethyloxycarbamate; GPCR, G-protein-coupled receptor; HEK 293 cells, human embryonic kidney 293 cells; MALDI-TOF, matrix-assisted laser desorption/ionization–time of flight; NMR, nuclear magnetic resonance; NOESY, nuclear Overhauser enhancement spectroscopy; RP-HPLC, reverse-phase high-performance liquid chromatography; TOCSY, total correlated spectroscopy; TSP, 3-(trimethylsilanyl)propionic acid; UII, urotensin II; URP, urotensin II-related peptide; UT, urotensin II receptor.

References

1. Vaudry, H., Leprince, J., Chatenet, D., Fournier, A., Lambert, D. G., Le Mevel, J. C., Ohlstein, E. H., Schwertani, A., Tostivint, H., and Vaudry, D. (2015) International Union of Basic and Clinical Pharmacology. XCII. Urotensin II, urotensin II-related peptide, and their receptor: From structure to function. *Pharmacol. Rev.* **67**, 214–258
2. Nassour, H., Iddir, M., and Chatenet, D. (2019) Towards targeting the urotensinergic system: Overview and challenges. *Trends Pharmacol. Sci.* **40**, 725–734
3. Watson, A. M., Olukman, M., Koulis, C., Tu, Y., Samijono, D., Yuen, D., Lee, C., Behm, D. J., Cooper, M. E., Jandeleit-Dahm, K. A., Calkin, A. C., and Allen, T. J. (2013) Urotensin II receptor antagonism confers vasoprotective effects in diabetes associated atherosclerosis: Studies in humans and in a mouse model of diabetes. *Diabetologia* **56**, 1155–1165
4. You, Z., Genest, J., Jr., Barrette, P. O., Hafiane, A., Behm, D. J., D'Orleans-Juste, P., and Schwertani, A. G. (2012) Genetic and pharmacological manipulation of urotensin II ameliorate the metabolic and atherosclerosis sequalae in mice. *Arterioscler. Thromb. Vasc. Biol.* **32**, 1809–1816
5. Zhao, J., Xie, L. D., Song, C. J., Mao, X. X., Yu, H. R., Yu, Q. X., Ren, L. Q., Shi, Y., Xie, Y. Q., Li, Y., Liu, S. S., and Yang, X. H. (2014) Urantide improves atherosclerosis by controlling C-reactive protein, monocyte chemotactic protein-1 and transforming growth factor-beta expression in rats. *Exp. Ther. Med.* **7**, 1647–1652
6. Zhao, J., Yu, Q. X., Kong, W., Gao, H. C., Sun, B., Xie, Y. Q., and Ren, L. Q. (2013) The urotensin II receptor antagonist, urantide, protects against atherosclerosis in rats. *Exp. Ther. Med.* **5**, 1765–1769
7. Lee, J. H., Park, B. K., Oh, K. S., Yi, K. Y., Lim, C. J., Seo, H. W., and Lee, B. H. (2016) A urotensin II receptor antagonist, KR36676, decreases vascular remodeling and inflammation in experimental pulmonary hypertension. *Int. Immunopharmacol.* **40**, 196–202
8. Pehlivan, Y., Dokuyucu, R., Demir, T., Kaplan, D. S., Koc, I., Orkmez, M., Turkbeyler, I. H., Ceribasi, A. O., Tutar, E., Taysi, S., Kisacik, B., and Onat, A. M. (2014) Palosuran treatment effective as bosentan in the treatment model of pulmonary arterial hypertension. *Inflammation* **37**, 1280–1288
9. Wang, Y., Tian, W., Xiu, C., Yan, M., Wang, S., and Mei, Y. (2019) Urantide improves the structure and function of right ventricle as determined by echocardiography in monocrotaline-induced pulmonary hypertension rat model. *Clin. Rheumatol.* **38**, 29–35
10. Bousette, N., Hu, F., Ohlstein, E. H., Dhanak, D., Douglas, S. A., and Giaid, A. (2006) Urotensin-II blockade with SB-611812 attenuates cardiac dysfunction in a rat model of coronary artery ligation. *J. Mol. Cell Cardiol.* **41**, 285–295
11. Bousette, N., Pottinger, J., Ramli, W., Ohlstein, E. H., Dhanak, D., Douglas, S. A., and Giaid, A. (2006) Urotensin-II receptor blockade with SB-611812 attenuates cardiac remodeling in experimental ischemic heart disease. *Peptides* **27**, 2919–2926
12. Oh, K. S., Lee, J. H., Yi, K. Y., Lim, C. J., Park, B. K., Seo, H. W., and Lee, B. H. (2017) A novel urotensin II receptor antagonist, KR-36996, improved cardiac function and attenuated cardiac hypertrophy in experimental heart failure. *Eur. J. Pharmacol.* **799**, 94–102
13. Billard, E., Iddir, M., Nassour, H., Lee-Gosselin, L., Poujol de Molliens, M., and Chatenet, D. (2018) New directions for urotensin II receptor ligands. *Pept. Sci.*, e24056
14. Kim, S. K., Li, Y., Park, C., Abrol, R., and Goddard, W. A., 3rd. (2010) Prediction of the three-dimensional structure for the rat urotensin II receptor, and comparison of the antagonist binding sites and binding selectivity between human and rat receptors from atomistic simulations. *ChemMedChem* **5**, 1594–1608
15. Brancaccio, D., Merlino, F., Limatola, A., Yousif, A. M., Gomez-Monterrey, I., Campiglia, P., Novellino, E., Grieco, P., and Carotenuto, A. (2015) An investigation into the origin of the biased agonism associated with the urotensin II receptor activation. *J. Pept. Sci.* **21**, 392–399
16. Merlino, F., Billard, E., Yousif, A. M., Di Maro, S., Brancaccio, D., Abate, L., Carotenuto, A., Bellavita, R., d'Emmanuele di Villa Bianca, R., Santicioli, P., Marinelli, L., Novellino, E., Hebert, T. E., Lubell, W. D., Chatenet, D., *et al.* (2019) Functional selectivity revealed by N-methylation scanning of human urotensin II and related peptides. *J. Med. Chem.* **62**, 1455–1467
17. Chatenet, D., Letourneau, M., Nguyen, Q. T., Doan, N. D., Dupuis, J., and Fournier, A. (2013) Discovery of new antagonists aimed at discriminating UII and URP-mediated biological activities: Insight into UII and URP receptor activation. *Br. J. Pharmacol.* **168**, 807–821
18. Chatenet, D., Nguyen, Q. T., Letourneau, M., Dupuis, J., and Fournier, A. (2012) Urocontrin, a novel UT receptor ligand with a unique pharmacological profile. *Biochem. Pharmacol.* **83**, 608–615
19. Doan, N. D., Nguyen, T. T., Letourneau, M., Turcotte, K., Fournier, A., and Chatenet, D. (2012) Biochemical and pharmacological characterization of nuclear urotensin-II binding sites in rat heart. *Br. J. Pharmacol.* **166**, 243–257
20. Jarry, M., Diallo, M., Lecointre, C., Desrues, L., Tokay, T., Chatenet, D., Leprince, J., Rossi, O., Vaudry, H., Tonon, M. C., Prezeau, L., Castel, H., and Gandolfo, P. (2010) The vasoactive peptides urotensin II and urotensin II-related peptide regulate astrocyte activity through common and distinct mechanisms: Involvement in cell proliferation. *Biochem. J.* **428**, 113–124
21. Prosser, H. C., Forster, M. E., Richards, A. M., and Pemberton, C. J. (2008) Urotensin II and urotensin II-related peptide (URP) in cardiac ischemia-reperfusion injury. *Peptides* **29**, 770–777
22. Billard, E., Hebert, T. E., and Chatenet, D. (2018) Discovery of new allosteric modulators of the urotensinergic system through substitution of the urotensin II-related peptide (URP) phenylalanine residue. *J. Med. Chem.* **61**, 8707–8716
23. Billard, E., Letourneau, M., Hebert, T. E., and Chatenet, D. (2017) Insight into the role of urotensin II-related peptide tyrosine residue in UT activation. *Biochem. Pharmacol.*, 100–107
24. Douchez, A., Billard, E., Hebert, T. E., Chatenet, D., and Lubell, W. D. (2017) Design, synthesis, and biological assessment of biased allosteric modulation of the urotensin II receptor using achiral 1,3,4-Benzotriazepin-2-one turn mimics. *J. Med. Chem.* **60**, 9838–9859
25. Dufour-Gallant, J., Chatenet, D., and Lubell, W. D. (2015) De novo conception of small molecule modulators based on endogenous peptide ligands: Pyrrolodiazepin-2-one gamma-turn mimics that differentially modulate urotensin II receptor-mediated vasoconstriction ex vivo. *J. Med. Chem.* **58**, 4624–4637
26. Merlino, F., Yousif, A. M., Billard, E., Dufour-Gallant, J., Turcotte, S., Grieco, P., Chatenet, D., and Lubell, W. D. (2016) Urotensin II((4-11)) azasulfuryl peptides: Synthesis and biological activity. *J. Med. Chem.* **59**, 4740–4752
27. Strack, M., Billard, E., Chatenet, D., and Lubell, W. D. (2017) Urotensin core mimics that modulate the biological activity of urotensin-II related peptide but not urotensin-II. *Bioorg. Med. Chem. Lett.* **27**, 3412–3416
28. Kenakin, T. (2012) The potential for selective pharmacological therapies through biased receptor signaling. *BMC Pharmacol. Toxicol.* **13**, 3
29. Kenakin, T. (2011) Functional selectivity and biased receptor signaling. *J. Pharmacol. Exp. Ther.* **336**, 296–302
30. Chaturvedi, M., Schilling, J., Beautrait, A., Bouvier, M., Benovic, J. L., and Shukla, A. K. (2018) Emerging paradigm of intracellular targeting of G protein-coupled receptors. *Trends Biochem. Sci.* **43**, 533–546

31. Dimond, P., Carlson, K., Bouvier, M., Gerard, C., Xu, L., Covic, L., Agarwal, A., Ernst, O. P., Janz, J. M., Schwartz, T. W., Gardella, T. J., Milligan, G., Kuliopulos, A., Sakmar, T. P., and Hunt, S. W., 3rd. (2011) G protein-coupled receptor modulation with pepducins: Moving closer to the clinic. *Ann. N. Y. Acad. Sci.* **1226**, 34–49
32. Carlson, K., McMurry, T., and Hunt, S. W., 3rd. (2012) Pepducins: Lipopeptide allosteric modulators of GPCR signaling. *Drug Discovery Today. Tech.* **9**, e1–e70
33. Covic, L., Gresser, A. L., Talavera, J., Swift, S., and Kuliopulos, A. (2002) Activation and inhibition of G protein-coupled receptors by cell-penetrating membrane-tethered peptides. *Proc. Natl. Acad. Sci. U. S. A.* **99**, 643–648
34. Covic, L., Misra, M., Badar, J., Singh, C., and Kuliopulos, A. (2002) Pepducin-based intervention of thrombin-receptor signaling and systemic platelet activation. *Nat. Med.* **8**, 1161–1165
35. Kaneider, N. C., Agarwal, A., Leger, A. J., and Kuliopulos, A. (2005) Reversing systemic inflammatory response syndrome with chemokine receptor pepducins. *Nat. Med.* **11**, 661–665
36. Quoyer, J., Janz, J. M., Luo, J., Ren, Y., Armando, S., Lukashova, V., Benovic, J. L., Carlson, K. E., Hunt, S. W., 3rd, and Bouvier, M. (2013) Pepducin targeting the C-X-C chemokine receptor type 4 acts as a biased agonist favoring activation of the inhibitory G protein. *Proc. Natl. Acad. Sci. U. S. A.* **110**, E5088–5097
37. Carr, R., 3rd, Du, Y., Quoyer, J., Panettieri, R. A., Jr., Janz, J. M., Bouvier, M., Kobilka, B. K., and Benovic, J. L. (2014) Development and characterization of pepducins as Gs-biased allosteric agonists. *J. Biol. Chem.* **289**, 35668–35684
38. Tressel, S. L., Koukos, G., Tchernychev, B., Jacques, S. L., Covic, L., and Kuliopulos, A. (2011) Pharmacology, biodistribution, and efficacy of GPCR-based pepducins in disease models. *Methods Mol. Biol.* **683**, 259–275
39. O'Callaghan, K., Kuliopulos, A., and Covic, L. (2012) Turning receptors on and off with intracellular pepducins: New insights into G-protein-coupled receptor drug development. *J. Biol. Chem.* **287**, 12787–12796
40. Saviello, M. R., Malfi, S., Campiglia, P., Cavalli, A., Grieco, P., Novellino, E., and Carotenuto, A. (2010) New insight into the mechanism of action of the temporin antimicrobial peptides. *Biochemistry* **49**, 1477–1485
41. Doreleijers, J. F., Rullmann, J. A., and Kaptein, R. (1998) Quality assessment of NMR structures: A statistical survey. *J. Mol. Biol.* **281**, 149–164
42. Zhang, P., Leger, A. J., Baleja, J. D., Rana, R., Corlin, T., Nguyen, N., Koukos, G., Bohm, A., Covic, L., and Kuliopulos, A. (2015) Allosteric activation of a G protein-coupled receptor with cell-penetrating receptor mimetics. *J. Biol. Chem.* **290**, 15785–15798
43. Brule, C., Perzo, N., Joubert, J. E., Sainsily, X., Leduc, R., Castel, H., and Prezeau, L. (2014) Biased signaling regulates the pleiotropic effects of the urotensin II receptor to modulate its cellular behaviors. *FASEB J.* **28**, 5148–5162
44. Lukasheva, V., Devost, D., Le Gouill, C., Namkung, Y., Martin, R. D., Longpre, J. M., Amraei, M., Shinjo, Y., Hogue, M., Lagace, M., Breton, B., Aoki, J., Tanny, J. C., Laporte, S. A., Pineyro, G., *et al.* (2020) Signal profiling of the beta1AR reveals coupling to novel signalling pathways and distinct phenotypic responses mediated by beta1AR and beta2AR. *Sci. Rep.* **10**, 8779
45. He, Y. H., Hong, J. M., Guo, H. S., Wei, J. R., Chen, H., Zuo, H. H., and Li, Z. L. (2004) [Effects of urotensin II on cultured cardiac fibroblast proliferation and collagen type I mRNA expression]. *Di Yi Jun Yi Da Xue Xue Bao* **24**, 505–508
46. Zhang, Y. G., Li, J., Li, Y. G., and Wei, R. H. (2008) Urotensin II induces phenotypic differentiation, migration, and collagen synthesis of adventitial fibroblasts from rat aorta. *J. Hypertens.* **26**, 1119–1126
47. Sauzeau, V., Le Mellionnec, E., Bertoglio, J., Scalbert, E., Pacaud, P., and Loirand, G. (2001) Human urotensin II-induced contraction and arterial smooth muscle cell proliferation are mediated by RhoA and Rho-kinase. *Circ. Res.* **88**, 1102–1104
48. Luttrell, L. M., Maudsley, S., and Bohn, L. M. (2015) Fulfilling the promise of "biased" G protein-coupled receptor agonism. *Mol. Pharmacol.* **88**, 579–588
49. Gurbel, P. A., Bliden, K. P., Turner, S. E., Tantry, U. S., Gesheff, M. G., Barr, T. P., Covic, L., and Kuliopulos, A. (2016) Cell-penetrating pepducin therapy targeting PAR1 in subjects with coronary artery disease. *Arterioscler. Thromb. Vasc. Biol.* **36**, 189–197
50. Armstrong, C. W. D., Coulter, J. A., Ong, C. W., Maxwell, P. J., Walker, S., Butterworth, K. T., Lyubomska, O., Berlingeri, S., Gallagher, R., O'Sullivan, J. M., Jain, S., Mills, I. G., Prise, K. M., Bristow, R. G., LaBonte, M. J., *et al.* (2020) Clinical and functional characterization of CXCR1/CXCR2 biology in the relapse and radiotherapy resistance of primary PTEN-deficient prostate carcinoma. *NAR Cancer* **2**, zcaa012
51. Kuliopulos, A., Gurbel, P. A., Rade, J. J., Kimmelstiel, C. D., Turner, S. E., Bliden, K. P., Fletcher, E. K., Cox, D. H., and Covic, L. (2020) PAR1 (Protease-Activated receptor 1) pepducin therapy targeting myocardial necrosis in coronary artery disease and acute coronary syndrome patients undergoing cardiac catheterization: A randomized, placebo-controlled, phase 2 study. *Arterioscler. Thromb. Vasc. Biol.* **40**, 2990–3003
52. Carr, R., 3rd, and Benovic, J. L. (2016) From biased signalling to polypharmacology: Unlocking unique intracellular signalling using pepducins. *Biochem. Soc. Trans.* **44**, 555–561
53. Buch, T. R., Biebermann, H., Kalwa, H., Pinkenburg, O., Hager, D., Barth, H., Aktories, K., Breit, A., and Gudermann, T. (2008) G13-dependent activation of MAPK by thyrotropin. *J. Biol. Chem.* **283**, 20330–20341
54. Goldsmith, Z. G., and Dhanasekaran, D. N. (2007) G protein regulation of MAPK networks. *Oncogene* **26**, 3122–3142
55. Hains, M. D., Wing, M. R., Maddileti, S., Siderovski, D. P., and Harden, T. K. (2006) Galpha12/13- and rho-dependent activation of phospholipase C-epsilon by lysophosphatidic acid and thrombin receptors. *Mol. Pharmacol.* **69**, 2068–2075
56. Mariggio, S., Bavec, A., Natale, E., Zizza, P., Salmona, M., Corda, D., and Di Girolamo, M. (2006) Galpha13 mediates activation of the cytosolic phospholipase A2alpha through fine regulation of ERK phosphorylation. *Cell Signal.* **18**, 2200–2208
57. Fan, G. H., Zhou, T. H., Zhang, W. B., and Pei, G. (1998) Suppression of phospholipase C blocks Gi-mediated inhibition of adenylyl cyclase activity. *Eur. J. Pharmacol.* **341**, 317–322
58. Wu, Y. L., Pei, G., and Fan, G. H. (1998) Inhibition of phospholipase C blocks opioid receptor-mediated activation of Gi proteins. *Neuroreport* **9**, 99–103
59. Belcheva, M. M., and Coscia, C. J. (2002) Diversity of G protein-coupled receptor signaling pathways to ERK/MAP kinase. *Neurosignals* **11**, 34–44
60. Blaukat, A., Barac, A., Cross, M. J., Offermanns, S., and Dikic, I. (2000) G protein-coupled receptor-mediated mitogen-activated protein kinase activation through cooperation of Galpha(q) and Galpha(i) signals. *Mol. Cell Biol.* **20**, 6837–6848
61. Handlogten, M. E., Huang, C., Shiraishi, N., Awata, H., and Miller, R. T. (2001) The Ca2+-sensing receptor activates cytosolic phospholipase A2 via a Gqalpha -dependent ERK-independent pathway. *J. Biol. Chem.* **276**, 13941–13948
62. Oduori, O. S., Murao, N., Shimomura, K., Takahashi, H., Zhang, Q., Dou, H., Sakai, S., Minami, K., Chanclon, B., Guida, C., Kothegala, L., Tolo, J., Maejima, Y., Yokoi, N., Minami, Y., *et al.* (2020) Gs/Gq signaling switch in beta cells defines incretin effectiveness in diabetes. *J. Clin. Invest.* **130**, 6639–6655
63. Esposito, G., Perrino, C., Cannavo, A., Schiattarella, G. G., Borgia, F., Sannino, A., Pironti, G., Gargiulo, G., Di Serafino, L., Franzone, A., Scudiero, L., Grieco, P., Indolfi, C., and Chiariello, M. (2011) EGFR transactivation by urotensin II receptor is mediated by beta-arrestin recruitment and confers cardioprotection in pressure overload-induced cardiac hypertrophy. *Basic Res. Cardiol.* **106**, 577–589
64. Grundmann, M., Merten, N., Malfacini, D., Inoue, A., Preis, P., Simon, K., Ruttiger, N., Ziegler, N., Benkel, T., Schmitt, N. K., Ishida, S., Muller, I., Reher, R., Kawakami, K., Inoue, A., *et al.* (2018) Lack of beta-arrestin signaling in the absence of active G proteins. *Nat. Commun.* **9**, 341
65. Gohla, A., Harhammer, R., and Schultz, G. (1998) The G-protein G13 but not G12 mediates signaling from lysophosphatidic acid receptor via epidermal growth factor receptor to Rho. *J. Biol. Chem.* **273**, 4653–4659
66. Kobilka, B. K., and Deupi, X. (2007) Conformational complexity of G-protein-coupled receptors. *Trends Pharmacol. Sci.* **28**, 397–406

67. Devost, D., Sleno, R., Petrin, D., Zhang, A., Shinjo, Y., Okde, R., Aoki, J., Inoue, A., and Hebert, T. E. (2017) Conformational profiling of the AT1 angiotensin II receptor reflects biased agonism, G protein coupling, and cellular context. *J. Biol. Chem.* **292**, 5443–5456
68. Granier, S., and Kobilka, B. (2012) A new era of GPCR structural and chemical biology. *Nat. Chem. Biol.* **8**, 670–673
69. Tsuji, M., Ueda, S., Hirayama, T., Okuda, K., Sakaguchi, Y., Isono, A., and Nagasawa, H. (2013) FRET-based imaging of transbilayer movement of pepducin in living cells by novel intracellular bioreductively activatable fluorescent probes. *Org. Biomol. Chem.* **11**, 3030–3037
70. Hwang, T. L., and Shaka, A. J. (1995) Water suppression that works. Excitation sculpting using arbitrary wave-forms and pulsed-field gradients. *J. Magn. Reson.* **112**, 275–279
71. Marion, D., and Wuthrich, K. (1983) Application of phase sensitive two-dimensional correlated spectroscopy (COSY) for measurements of 1H-1H spin-spin coupling constants in proteins. *Biochem. Biophys. Res. Commun.* **113**, 967–974
72. Piantini, U., Sorensen, O. W., and Ernst, R. R. (1982) Multiple quantum filters for elucidating NMR coupling network. *J. Am. Chem. Soc.* **104**, 6800–6801
73. Braunschweiler, L., and Ernst, R. R. (1983) Coherence transfer by isotropic mixing: Application to proton correlation spectroscopy. *J. Magn. Res.* **53**, 521–528
74. Jenner, J., Meyer, B. H., Bachman, P., and Ernst, R. R. (1979) Investigation of exchange processes by two-dimensional NMR spectroscopy. *J. Chem. Phys.* **71**, 4546–4553
75. States, D. J., Haberkorn, R. A., and Ruben, D. J. (1982) A two-dimensional nuclear overhauser ex-periment with pure absorption phase in four quadrants. *J. Magn. Reson.* **42**, 286–292
76. Bartels, C., Xia, T., Billeter, M., Guentert, P., and Wüthrich, K. (1995) The program XEASY for com-puter-supported NMR spectral analysis of biological macromolecules. *J. Biomol. NMR* **6**, 1–10
77. Wüthrich, K. (1986) *NMR of Proteins and Nucleic Acids*, John Wiley & Sons, New York, NY
78. Guntert, P., Mumenthaler, C., and Wuthrich, K. (1997) Torsion angle dynamics for NMR structure calculation with the new program DYANA. *J. Mol. Biol.* **273**, 283–298
79. Maple, J. R., Dinur, U., and Hagler, A. T. (1988) Derivation of force fields for molecular mechanics and dynamics from *ab initio* energy surfaces. *Proc. Natl. Acad. Sci. U. S. A.* **85**, 5350–5354
80. Pettersen, E. F., Goddard, T. D., Huang, C. C., Couch, G. S., Greenblatt, D. M., Meng, E. C., and Ferrin, T. E. (2004) UCSF Chimera–a visualization system for exploratory research and analysis. *J. Comput. Chem.* **25**, 1605–1612
81. Breton, B., Sauvageau, E., Zhou, J., Bonin, H., Le Gouill, C., and Bouvier, M. (2010) Multiplexing of multicolor bioluminescence resonance energy transfer. *Biophys. J.* **99**, 4037–4046
82. Zhang, Y. G., Li, Y. G., Liu, B. G., Wei, R. H., Wang, D. M., Tan, X. R., Bu, D. F., Pang, Y. Z., and Tang, C. S. (2007) Urotensin II accelerates cardiac fibrosis and hypertrophy of rats induced by isoproterenol. *Acta Pharmacol. Sin* **28**, 36–43
83. Colombo, F., Gosselin, H., El-Helou, V., and Calderone, A. (2003) Beta-adrenergic receptor-mediated DNA synthesis in neonatal rat cardiac fibroblasts proceeds via a phosphatidylinositol 3-kinase dependent pathway refractory to the antiproliferative action of cyclic AMP. *J. Cell Physiol.* **195**, 322–330
84. Andersen, N. H., Liu, Z., and Prickett, K. S. (1996) Efforts toward deriving the CD spectrum of a 3(10) helix in aqueous medium. *FEBS Lett.* **399**, 47–52